1973

Application of a theoretical model to velocity fields observed over water waves.

Stauffer, Barry C.

Monterey, California. Naval Postgraduate School

APPLICATION OF A THEORETICAL MODEL TO VELOCITY FIELDS OBSERVED OVER WATER WAVES

Barry C. Stauffer

NAVAL POSTGRADUATE SCHOOL
Monterey, California

THESIS

APPLICATION OF A THEORETICAL MODEL TO VELOCITY FIELDS OBSERVED OVER WATER WAVES

by

Barry C. Stauffer

Thesis Advisor: R. T. Williams

March 1973

Approved for public release; distribution unlimited.

Application of a Theoretical Model to Velocity Fields Observed Over Water Waves

by

Barry C. Stauffer
Lieutenant Commander, United States Navy
B.S., Pennsylvania State University, 1963

Submitted in partial fulfillment of the
requirements for the degree of

MASTER OF SCIENCE IN METEOROLOGY

from the

NAVAL POSTGRADUATE SCHOOL
March 1973

ABSTRACT

A theoretical model is developed for the wind velocity field in the atmospheric near-water layer above ocean waves. A turbulent exchange coefficient due to the wave-caused velocity fluctuations is introduced into the equations to account for the corresponding turbulent nature of the motion and the resulting energy fluxes. The equations of motion for air are derived in a manner to allow for variation of the turbulent exchange coefficient with height. A stream function is introduced and a numerical solution obtained by utilization of the Richtmyer method. The profiles of wave-caused Reynolds stresses and their resulting energy transfers are discussed and compared with observational data.

TABLE OF CONTENTS

LIST OF TABLES

LIST OF FIGURES

TABLE OF SYMBOLS AND ABBREVIATIONS

A - stream function amplitude (cosine coefficient)

a - wave amplitude

B - stream function amplitude (sine coefficient)

C - phase speed

Fs - scaling factor for the velocities

Fq - scaling factor for the stresses

G - acceleration of gravity

H - height of the boundary layer

K - coefficient of turbulent exchange which is related to the mean velocity gradient

k - wave number

κ - von-Karmans constant ($\kappa = 0.35$)

λ - wavelength

ν - coefficient of turbulent exchange associated with the wave-caused velocity fluctuations

ν_m - coefficient of molecular viscosity

P - pressure

t - time

τ - Reynolds stress (m^2/sec^2)

U - mean horizontal velocity

u - total velocity

u' - turbulent velocity fluctuation

U_* - dynamic velocity

W - total wind

w - vertical velocity

ψ - stream function

ψ_c - stationary portion of the stream function

z - height

ζ - vorticity ($\nabla^2\psi$)

ACKNOWLEDGEMENTS

I wish to express my deep gratitude to Dr. R. Terry Williams for his patient guidance, encouragement and advice. Without his help, this research would have been much more perplexing and much more difficult.

My appreciation is extended to Dr. K. L. Davidson and Lieutenant Commander A. J. Frank for the use of their data which was used for the comparisons with the numerical results.

The computations were accomplished at the W. R. Church Computer Center, Naval Postgraduate School, Monterey, California. The advice of the computer center personnel and their cheerful assistance is greatly appreciated.

I also want to thank my wife, Audrey, whose steadfast support, moral encouragement and selflessness made this thesis possible.

I. INTRODUCTION

Energy and momentum transfer to water waves are primarily dependent upon the conditions of the atmosphere immediately adjacent to the ocean surface. In the case of air flow above an open body of water the atmosphere-ocean interactions give rise to wave perturbations in the upper layer of the water and in the adjacent atmosphere. It has been suggested that the wave perturbation characteristics be used to determine the energy and momentum transfers across the air-sea boundary.

Investigation of the nature of these energy and momentum transfers have been the purpose of numerous studies in recent years. Such studies of wind-wave coupling were initiated with the quasi-laminar model of Miles (1957), who allowed the wave-induced motion to interact with the shear flow only at the critical level. Models progressed through the studies of Phillips (1957) and Benjamin (1958) to those more recently of Yefimov (1970) and Reynolds (1972), wherein there is also interaction with the turbulent Reynolds stresses.

In the present study, wave related momentum transfers were investigated through the use of a numerical model. This study is similar to that of Yefimov (1970), but it is more general and allows for dependence of the mean wind on time and variation of the turbulent coefficient with

height. This model utilizes an initial value numerical procedure similar to that of Newman (1969).

In addition, specific data derived from the statistical study of Davidson and Frank (1973) will be utilized to define solution parameters to generate the numerically derived stress patterns.

II. FORMULATION OF THE MODEL

The basis of the problem is the equation of motion. Since the stress is expected to be independent of y, two-dimensional motion is assumed with the resulting equation in the form:

$$\frac{\partial \mathbb{W}}{\partial t} + \mathbb{W} \cdot \nabla \mathbb{W} = - \frac{1}{\rho} \nabla P + \mathbb{F}, \qquad (2.1)$$

where

$$F_x = \frac{\partial}{\partial x} (-\bar{u}'^2) + \frac{\partial}{\partial z} (\overline{u'w'}), \text{ and}$$

$$F_z = \frac{\partial}{\partial x} (-\overline{u'w'}) + \frac{\partial}{\partial z} (-\bar{w}'^2) .$$

Here x is the horizontal axis; z is the vertical axis; ρ is the density of air; P is the non-hydrostatic pressure; u' and w' are the turbulent velocity fluctuations. The stationary part of each variable (time average) will be denoted with a straight line above it and the nonstationary part (space average) by a waved line. The stationary velocities do not include the random components which would disappear with a suitable time average. The velocity ($\mathbb{W}$) will be defined as:

$$\mathbb{W} = (u + U)\, \mathbb{i} + w\, \mathbb{k}, \qquad (2.2)$$

where $U = U(z)$ and the factor $\frac{\partial U}{\partial t}$ will be neglected in the development of the equations. For simplicity the problem will be restricted to those cases of a single wave number. This neglects the effect of wave self-interaction which would affect other waves.

The turbulent velocity fluctuations, u' and w' are assumed to have a dual nature. They are generated by the gradient of the mean velocity in the near water layer and also by the wave-caused perturbations of the velocity. The tangential Reynolds stress ($\overline{u'w'}$) will be expressed as:

$$\tau = -\overline{u'w'} = K \frac{\partial U}{\partial z} + \nu \left(\frac{\partial u}{\partial z} + \frac{\partial w}{\partial x}\right) , \qquad (2.3)$$

where u and w are the horizontal and vertical components of wave-caused velocity perturbations. The factor K is the coefficient of turbulent exchange which is related to the generation of turbulent fluctuations by the mean velocity gradient. The element ν is the coefficient of turbulent exchange which is related to the wave-caused velocity fluctuations. It will be assumed that $\nu >> \nu_m$ everywhere except in the thin laminar sublayer in which we shall neglect the effect of turbulent viscosity. Both the coefficients, K and ν, will be assumed to be constant in the x-direction and ν is a function of height. In addition, the coefficient K will be assumed to be given by:

$$K = \kappa U_* z$$

which increases linearly with height and leads to the undisturbed mean velocity profile

$$U = \frac{U_*}{\kappa} \ln \left(\frac{z}{z_o} + 1\right) . \qquad (2.4)$$

Incorporating the continuity equation with the Boussinesq approximation, $(\nabla \cdot \mathbb{V}) = 0$, the equations may be written in component form as:

$$\frac{\partial u}{\partial t} + \mathbb{V} \cdot \nabla u + w\frac{\partial U}{\partial z} = -\frac{1}{\rho}\frac{\partial P}{\partial x} + \frac{\partial}{\partial x}(-\overline{u'^2}) + \frac{\partial}{\partial z}[K\frac{\partial U}{\partial z} + \nu(\frac{\partial u}{\partial z} + \frac{\partial w}{\partial x})], \quad (2.5)$$

$$\frac{\partial w}{\partial z} + \mathbb{V} \cdot \nabla w = -\frac{1}{\rho}\frac{\partial P}{\partial z} + \frac{\partial}{\partial x}[K\frac{\partial U}{\partial z} + \nu(\frac{\partial u}{\partial z} + \frac{\partial w}{\partial x})] + \frac{\partial}{\partial z}(-\overline{w'^2}). \quad (2.6)$$

The vorticity (ζ) is defined to be:

$$\zeta = \frac{\partial u}{\partial z} - \frac{\partial w}{\partial x} .$$

Normally $\overline{u'^2} \doteq \frac{3}{2}\overline{w'^2}$ but for this work the assumption of:

$$\overline{u'^2} = \overline{w'^2}$$

will be incorporated into the vorticity equation which may now be written in the form:

$$\frac{\partial \zeta}{\partial t} + \mathbb{V} \cdot \nabla \zeta + \frac{\partial \mathbb{V}}{\partial z} \cdot \nabla u - \frac{\partial \mathbb{V}}{\partial x} \cdot \nabla w + \frac{\partial}{\partial z}(w\frac{\partial U}{\partial z}) =$$

$$\frac{\partial^2}{\partial z^2}[K\frac{\partial U}{\partial z} + \nu(\frac{\partial u}{\partial z} + \frac{\partial w}{\partial x})] - \nu[\frac{\partial^3 u}{\partial z^2 \partial z} + \frac{\partial^3 w}{\partial x^3}] \quad (2.7)$$

If the continuity equation,

$$\frac{\partial u}{\partial x} + \frac{\partial w}{\partial z} = 0 ,$$

is used, the vorticity equation becomes:

$$\frac{\partial \zeta}{\partial t} + U\frac{\partial \zeta}{\partial x} + w\frac{\partial^2 U}{\partial z^2} + u\frac{\partial \zeta}{\partial x} + w\frac{\partial \zeta}{\partial z} =$$

$$\frac{\partial^2}{\partial z^2}[K\frac{\partial U}{\partial z} + \nu(\frac{\partial u}{\partial z} + \frac{\partial w}{\partial x})] - \nu(\frac{\partial^3 u}{\partial x^2 \partial z} + \frac{\partial^3 w}{\partial x^3}) \quad (2.8)$$

The products of the perturbation quantities are neglected except where they affect the mean flow. This is consistent with the consideration of a single wave number.

The mean quantities are balanced separately and subtracted from (2.8). This results in the two-equation system:

$$\frac{\partial \zeta}{\partial t} + U\frac{\partial \zeta}{\partial x} + w\frac{\partial^2 U}{\partial z^2} = \frac{\partial^2}{\partial z^2}[\nu(\frac{\partial u}{\partial z} + \frac{\partial w}{\partial x})] - \nu[\frac{\partial^3 u}{\partial x^2 \partial z} + \frac{\partial^3 w}{\partial x^3}] \ , \qquad (2.9)$$

$$U\frac{\partial \tilde{\zeta}}{\partial x} + w\frac{\partial \tilde{\zeta}}{\partial z} = \frac{\partial^2}{\partial z^2}(K\frac{\partial U}{\partial z}) \ . \qquad (2.10)$$

With the introduction of stream function notation, the velocities can be defined as:

$$u = \frac{\partial \psi}{\partial z} \ , \quad w = -\frac{\partial \psi}{\partial x} \ , \qquad (2.11)$$

which transforms (2.9) and (2.10) into:

$$\frac{\partial}{\partial t}(\psi_{zz} + \psi_{xx}) = -U(\psi_{xzz} + \psi_{xxx}) + \psi_x U_{zz} + \frac{\partial}{\partial z^2}[\nu(\psi_{zz} - \psi_{xx})] - \nu[\psi_{xxzz} - \psi_{xxxx}] \ , \qquad (2.12)$$

$$\tilde{\psi}_z\tilde{\psi}_{xxx} + \tilde{\psi}_z\tilde{\psi}_{xzz} - \tilde{\psi}_x\tilde{\psi}_{zxx} - \tilde{\psi}_x\tilde{\psi}_{zzz} = \overline{K\psi}_{zzzz} \qquad (2.13)$$

Yefimov (1970) simplified the solution by assuming K and ν to be of the same order. This assumption will be incorporated into equation (2.13) by replacing K by ν.

The analytic solution for the special case, U = 0, to (2.12) and (2.13) has been considered by Yefimov and Pososhkov (1970). Their results have been adapted and incorporated as a test of the numerical technique as outlined in Appendix C.

The stream function will be defined as:

$$\psi = \psi_o(z,t) + A(z,t)\cos[k(x-ct)] + B(z,t)\sin[k(x-ct)] \quad (2.14)$$

where $A(z,t)$ and $B(z,t)$ are the stream function amplitudes.

Substitute the expressions for the various derivations of ψ into (2.12) and (2.13) and equate coefficients of the cosine terms to produce:

$$\frac{\partial}{\partial t}(A_{zz} - Ak^2) = (U-c)[Bk^3 - B_{zz}k] + BkU_{zz} + \frac{\partial^2}{\partial z^2}[\nu(A_{zz} + Ak^2)] + \nu[A_{zz}k^2 + Ak^4] . \quad (2.15)$$

The coefficients of the sine terms are:

$$\frac{\partial}{\partial t}(B_{zz} - Bk^2) = -(U-c)[Ak^3 - A_{zz}k] - AkU_{zz} + \frac{\partial^2}{\partial z^2}[\nu(B_{zz} + Bk^2)] + \nu[B_{zz}k^2 + Bk^4] . \quad (2.16)$$

The mean velocity equation is:

$$\frac{k}{2}[A_z B_{zz} - A_{zzz}B - A_{zz}B_z + AB_{zzz}] = \nu\psi_{ozzzz} \quad (2.17)$$

Equations (2.15) and (2.16) determine the wave-caused velocity perturbations and therefore are the basic equations for solving the problem. Equation (2.17) is used for the calculation of the mean velocity perturbation $\tilde{u}$.

III. SOLUTION OF THE PROBLEM

A. INITIALIZATION

To initiate the solution of equations (2.15) and (2.16), the undisturbed mean velocity was assumed to be in the form:

$$U(z) = \frac{U_*}{K} \ln \left(\frac{z}{z_o} + 1\right) , \qquad (3.1)$$

as shown in Figure 1.

The functions A(z,t) and B(z,t) were initialized through:

$$A(z,0) = A(0,0) \sinh [k(H1-z)]/\sinh(kH1), \qquad (3.2)$$

and

$$B(z,0) = 0 , \qquad (3.3)$$

where H is the height of the boundary layer and H1 the height one grid point less than H.

B. BOUNDARY CONDITIONS

Yefimov (1970) defined the boundary conditions for the lower boundary of the turbulent layer as:

$$u(0,t) = akc\cos[k(x-ct)],$$

$$w(0,t) = akc\sin[k(x-ct)].$$

In terms of the stream function the problem was solved with the boundary conditions:

$$A(0,t) = ac, \qquad A_z(0,t) = -akc, \qquad (3.4)$$

$$B(0,t) = B_z(0,t) = 0 , \qquad (3.5)$$

$$A(H,t) = A_z(H,t) = B(H,t) = B_z(H,t) = 0 . \qquad (3.6)$$

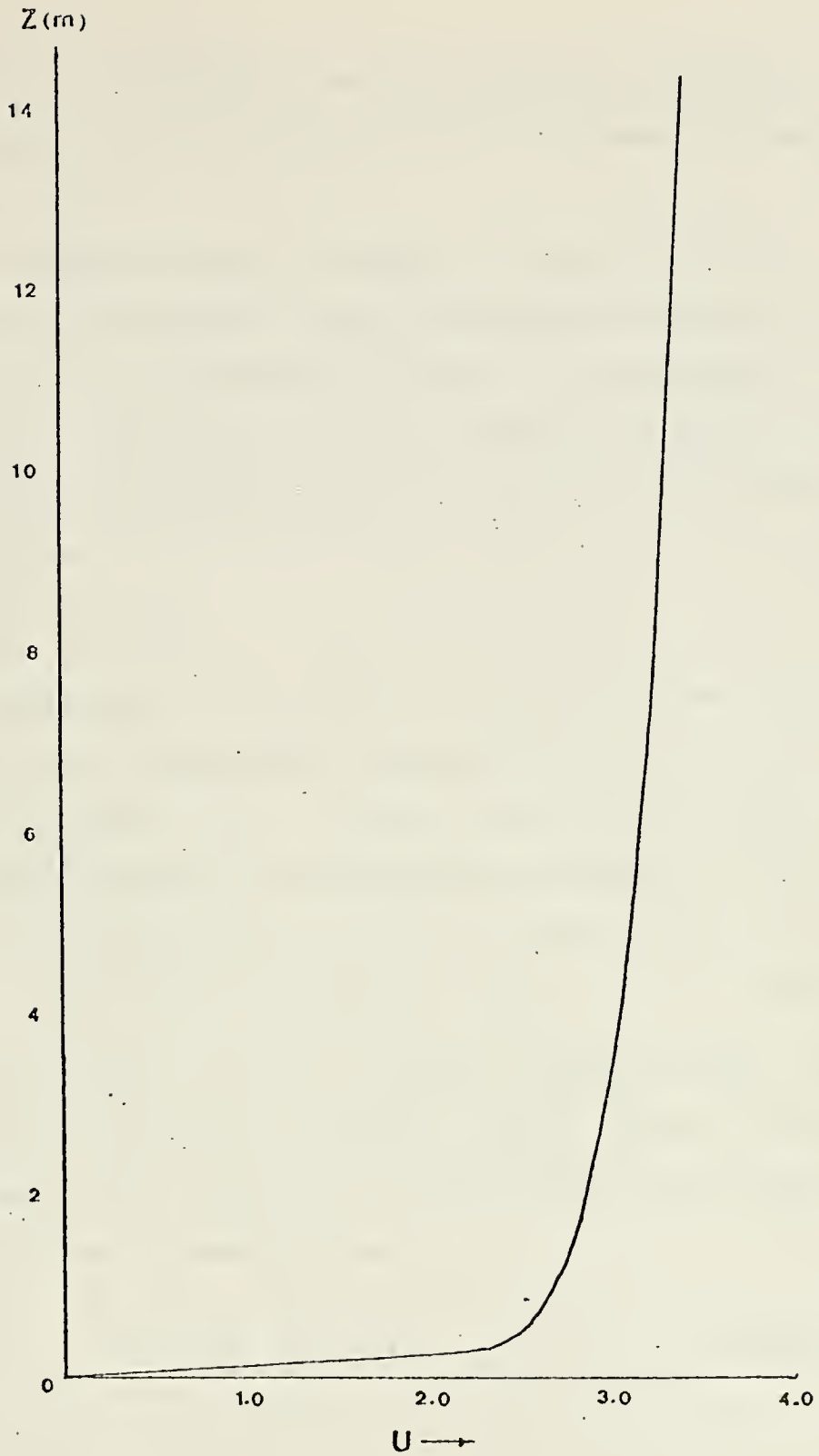

Figure 1. Undisturbed mean velocity profile (m/sec).

Consequently, the boundary layer was limited to a certain height H, where the wave-caused velocity perturbations were set equal to zero.

Yefimov (1970) studied a similar problem in which the upper limit of the boundary layer was chosen sufficiently high so that it was reasonable to assume the conditions of (3.6) to hold. This upper limit was found to be greater than one and one-half wavelengths in order to reach a stationary solution.

C. RESULTANT FACTORS

As a consequence of the initialization functions (3.1), (3.2) and (3.3); the boundary conditions (3.4), (3.5) and (3.6), the functions A(z,t) and B(z,t) were time stepped forward until a steady state solution was reached. At each time step the Reynolds wave stress was computed from:

$$\tau = -\overline{uw} = -\frac{1}{2}k\,(B_z A - A_z B). \qquad (3.7)$$

According to equation (2.17) a non-zero Reynolds stress will result in a mean horizontal velocity ($\tilde{u}$) of the wave-caused perturbations. This supplement to the initial undisturbed mean velocity may be computed as:

$$\tilde{u} = -\frac{1}{\nu}\int_0^H \tau\,dz \qquad (3.8)$$

and applied as a correction to U at each time step by:

$$U(t) = \frac{U_*}{\kappa} \ln \left(\frac{z}{z_o} + 1\right) + \tilde{u} \ . \qquad (3.9)$$

D. FINITE DIFFERENCING

The finite differencing was accomplished through the use of centered finite difference schemes for all terms except those involving friction. These terms were computed at time $(t-\Delta t)$. Examples of the schemes are:

$$A_z = \frac{1}{2} \Delta z \ (A_{K+1} - A_{K-1}) \ , \qquad (3.10)$$

and

$$A_{zz} = \frac{1}{\Delta z^2} \ (A_{K+1} - 2A_K + A_{K-1}) \ . \qquad (3.11)$$

As a result of the finite difference schemes and the boundary conditions, the variables at the second grid point are specified by:

$$B(\Delta z, t) = 0 \ .$$

In addition the difference schemes and the boundary conditions specify that the stream function amplitudes $A(z,t)$ and $B(z,t)$ remain constant at both the bottom and top two grid points.

E. NUMERICAL SOLUTION

Equations (2.15) and (2.16) were solved utilizing the principle of Richtmyer (1957) with a forward time step to start the marching procedure. To avoid solution separation, the problem was restarted every 50 time steps with a finite

difference scheme developed by Matsuno (1966). This was a two-step iteration to simulate the Euler backward difference method.

All calculations were performed to double precision accuracy and continued until the Reynolds stress (3.7) reached a steady state condition which is defined by:

$$R = \left(\sum_{o}^{H} [\tau(z,t) - \tau(z,t-1)]^2 \right)^{1/2} \leq 1 \times 10^{-5}.$$

A space step of 0.25 meters and a time step of 0.0125 seconds were utilized. Additional accuracy was attained in some cases by reducing the space step to 0.125 meters with a corresponding time step of 0.00312 seconds.

IV. COMPUTATIONAL PROCEDURES

A. VARIABLES

The forecast formulas, as stated in (2.15) and (2.16), allow for five independent variables. These are wave amplitude (a), wave number(k), dynamic velocity (U_*), roughness length (z_o), and the coefficient of turbulent exchange (ν).

Yefimov (1970) assumed that the slope of the waves was small, so that the expressions for the velocities on the boundary predicted by the theory of waves of small slope could be applied. This assumption of a small slope is applied by establishing the relationship ak = .01, which is incorporated in the model as a means of computing the initial wave amplitude A(0,0).

The resulting variables k, U_*, z_o, and ν were then considered systematically by first determining the range of variation of each of the variables. Then central values were selected and used as example cases by holding three variables fixed and computing test cases of the remaining variable over its full range.

Kraus (1967) studied the relationship of the roughness length to that of the mean wind where roughness length is given by:

$$z_o = \frac{m}{G} U_*^2 .$$

The constant, m, was determined by different researchers with values ranging from 0.0125 to 0.08. A central value of m = 0.042 was selected and the roughness length was computed from:

$$z_o = 0.00428\ U_*^2 \ , \qquad (4.1)$$

for the case where z_o was dependent upon U_*. This reduces the independent variables to U_*, k and ν.

The majority of the experiments were conducted with z_o = 0.0001 meters after Hill (1962).

B. MODEL CONSIDERATIONS

Although the value of the coefficient of turbulent exchange is unknown, it is reasonable to assume that it can be variable with height as discussed by Yefimov (1970). This possibility has been incorporated in the model and several cases have been investigated where ν was allowed to vary with height.

V. RESULTS

A. EXPERIMENTAL RESULTS

The number of variables and their large range of variation necessitated numerous numerical experiments. To reduce the number of experiments as much as possible, the variables were restricted to a limited range. The selection of a variation increment was guided by the necessity to choose a sufficiently large increment while remaining within the scope of full investigation of the problem. The variables and the range of values used are shown in Table 1. These were used in the various combinations as shown on Figures 2 - 10.

TABLE I. Range of the variables considered in the numerical experiments.

$k(m^{-1})$	U_*(m/sec)	$\nu(m^2/sec)$	z_o(m)
0.050	0.010	1.100	0.10
0.075	*0.020	*0.240	0.01
0.100	0.040	0.200	0.001
0.125	0.060	0.110	0.0005
0.150	0.080	0.020	*0.0001
0.175	*0.100	0.011	0.00005
*0.200	0.150	0.002	0.00001
0.225	*0.200		0.000005
0.250	0.250		0.000001
0.275	0.300		
0.300	0.350		
	0.400		

*central values

The existence of a critical level was an important factor in the determination of the profile of the solution. The critical level is defined as that height where phase speed is equal to the mean wind speed. Since the phase speed is inversely proportional to the wave number($c = \sqrt{G/k}$), the phase speed will decrease as wave number increases. Therefore, for a fixed mean wind profile, an increase in wave number will decrease the height of the critical level (if existing). In the cases of fixed wave numbers, an increase in U_*, or decrease of z_o should decrease the height of the critical level.

The first case considered was that of a variable wave number. In this case the results were greatly affected by the value chosen for U_* and therefore two experiments were conducted. In the first experiment (Figure 2) the wave number was varied with U_*= 0.20 m/sec. The second experiment (Figure 3) was identical but U_* = 0.020 m/sec.

Some noteworthy features of these two tests are:

a. the decrease in magnitude and variation of τ as U_* was decreased;

b. the decrease in magnitude and variation of τ as k was increased;

c. a maximum value of τ occurs at approximately one meter above the wave surface;

d. the increase in τ at a certain wave number when U_* = 0.20 m/sec. It is significant that this was the

first case in which the critical level was within the layer where τ varies significantly.

The second case considered was that of different mean wind profiles. The mean wind given by (3.1) is dependent upon by U_* and z_o. Since U_* and z_o are considered to be interrelated there are numerous ways to vary the mean wind profile. In this study three experiments were conducted. The first case (Figure 4) was that of a fixed wave number, roughness length and turbulent coefficient. In the second case (Figure 5) the wave number and turbulent coefficient remained fixed but the roughness length was allowed to vary according to (4.1). Hence, both dynamic velocity and roughness length varied in this case. The third case (Figure 6) was that of fixed dynamic velocity, wave number and turbulent coefficient, while roughness length was allowed to vary.

Some notable features are:

a. the increase in magnitude of the wave-related stress as z_o was decreased;

b. the increase in magnitude of the wave-related stress as U_* was increased until U_* is approximately equal to 0.25 m/sec. This is the point where the critical level is within the layer where τ varies significantly.

The third case to be considered was that of various turbulent coefficients (Figure 7) while the other variables were held fixed.

A noteworthy feature is the increase in magnitude of τ as ν decreased to 0.020 m^2/sec. This is followed by a decrease in the magnitude of τ as ν continued to decrease.

In the fourth case the turbulent coefficient was allowed to vary with height (Figure 8). In the first experiment the turbulent coefficient was decreased with height, to 10 meters, according to the relationship:

$$\nu(z) = 0.5 \sinh (H-z)/\sinh(H).$$

On the subsequent experiments ν increased linearly with height (Figure 8) until ν = 0.24 m^2/sec and then remained constant thereafter. The results of the first experiment are shown in Figure 9 and those of the increasing ν experiments are shown in Figure 10. A similar case, but with ν held constant, is shown in Figure 10 for comparison.

Some notable features are:

a. the similarity in the profiles of the cases of increasing ν with that of decreasing ν;

b. the presence of a maximum at approximately 0.5 meters above the wave surface;

c. the rapid change from positive to negative stress;

d. the decrease in magnitude of τ as ν increases to greater heights.

B. COMPARISONS WITH DATA

Additional experiments were conducted to compare the results of this model with that of the data analyzed by

Davidson and Frank (1973). The initial input parameters (Table II) were combined with a constant turbulent coefficient (ν = 0.240 m^2/sec) and the calculations time stepped forward until a steady state was reached. The resulting stress profiles and amplitudes are shown in Figures 11-13.

TABLE II. Dynamic velocity, wavelength and roughness length values determined by Davidson and Frank (1973) with corresponding wave numbers and critical levels.

Case	U_*(m/sec)	λ(m)	z_o(m)	k(m^{-1})	critical level(m)
1.	0.200	35	0.003280	0.179	43.50
2.	0.167	23	0.000079	0.273	29.00
3.	0.121	23	0.000130	0.273	none

Appendix E outlines the procedure for obtaining data from the reported results of Davidson and Frank (1973) and also the procedures for interpretation of the numerical results. The elements for comparison have been displayed in Table III.

A significant feature of Table III is the high-degree of correlation of the magnitude of the velocities obtained from the variance spectra, phase amplitude and numerical amplitude procedures. An equally significant feature is the correlation of the magnitude of the stresses obtained by the velocity cospectra with those from the numerical calculations. It should be noted that the sign of the cospectra stress is dependent upon the wave phase. The

differences in the signs should therefore not be considered as a significant discrepancy.

The comparisons are the first of this kind for data from the natural regime. The agreement is significant.

TABLE III. Comparison of the numerically derived results with statistically analyzed results from Davidson and Frank (1973).

Period	Height	Amplitude Comparisons						Stress Comparisons	
		Velocity Variance Spectra		Phase Amplitude		Numerical Amplitude*		Velocity co-spectra	Numerical stress+
	(m)	u'	w'	u'	w'	u'	w'	$\overline{u'w'}$	$\overline{u'w'}$
1	1.5	0.196	0.250	0.120	0.250	0.678	0.456	-0.00470	0.00587
1	4.0	0.231	0.211	0.050	0.130	0.284	0.270	0.00630	-0.00174
2	1.5	0.172	0.054	0.140	0.057	0.310	0.188	0.00523	0.00240
2	4.0	0.154	0.038	0.030	0.025	0.073	0.070	0.00523	-0.00239
3	1.0	0.172	0.128	0.250	0.210	0.274	0.215	0.00628	0.00196
3	2.0	0.158	0.163	0.170	0.130	0.181	0.154	-0.00312	-0.00097

*Normalized by equation (E4).

+Normalized by equation (E5).

Note: All velocity units are expressed in m/sec and all stress units in $(m/sec)^2$

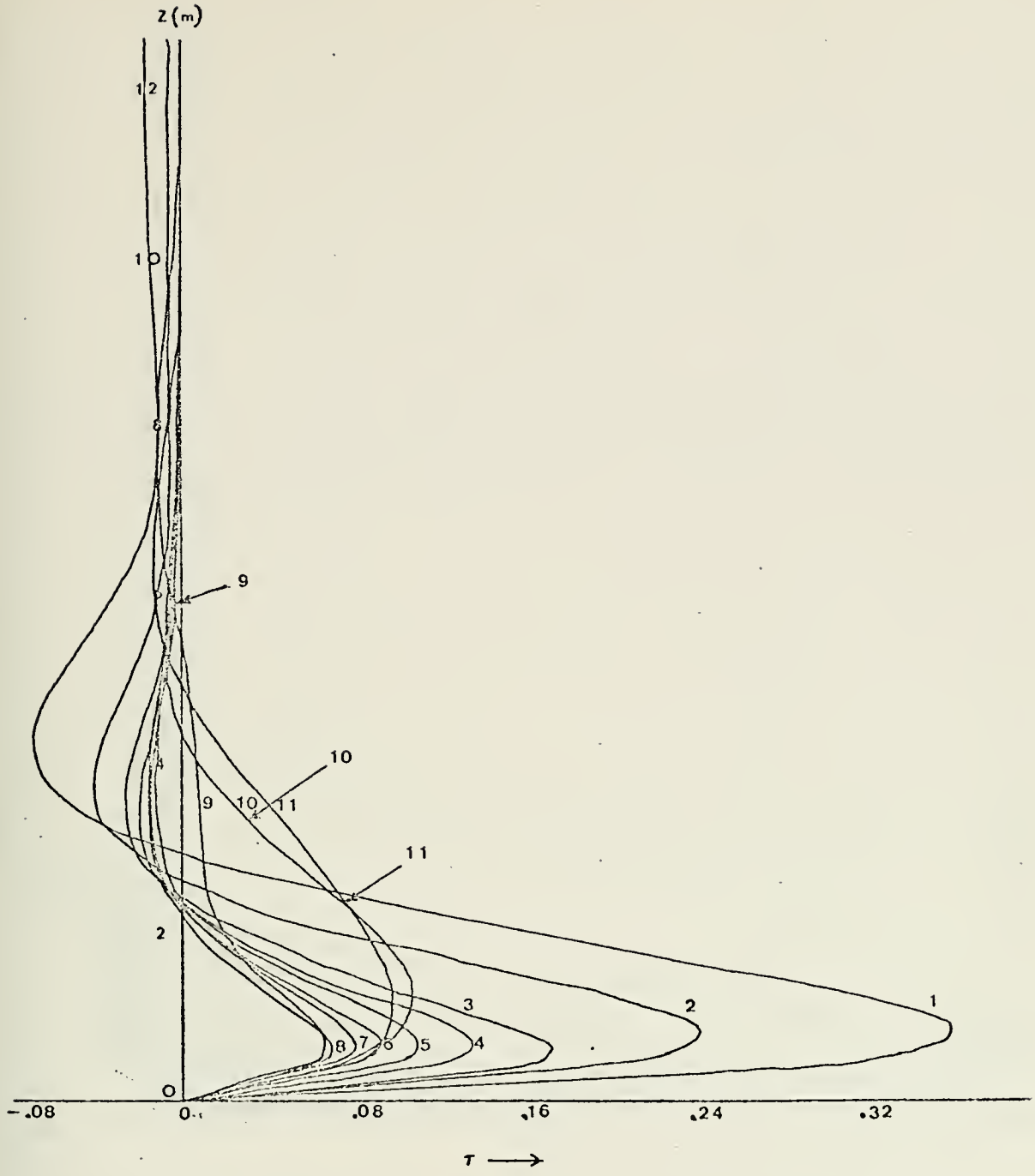

Figure 2. Distribution of the wave-caused stress (τ in m^2/sec^2) with height for $U_* = 0.2$ m/sec, $\nu = 0.240$ $m^2 sec^2$, $z_o = 0.0001$m and k equal, respectively, to: 1) 0.050, 2) 0.075, 3) 0.100, 4) 0.125, 5) 0.150, 6) 0.175, 7) 0.200, 8) 0.225, 9) 0.250, 10) 0.275, 11) 0.300. The arrows indicate the height of the critical level and the identifying wave number.

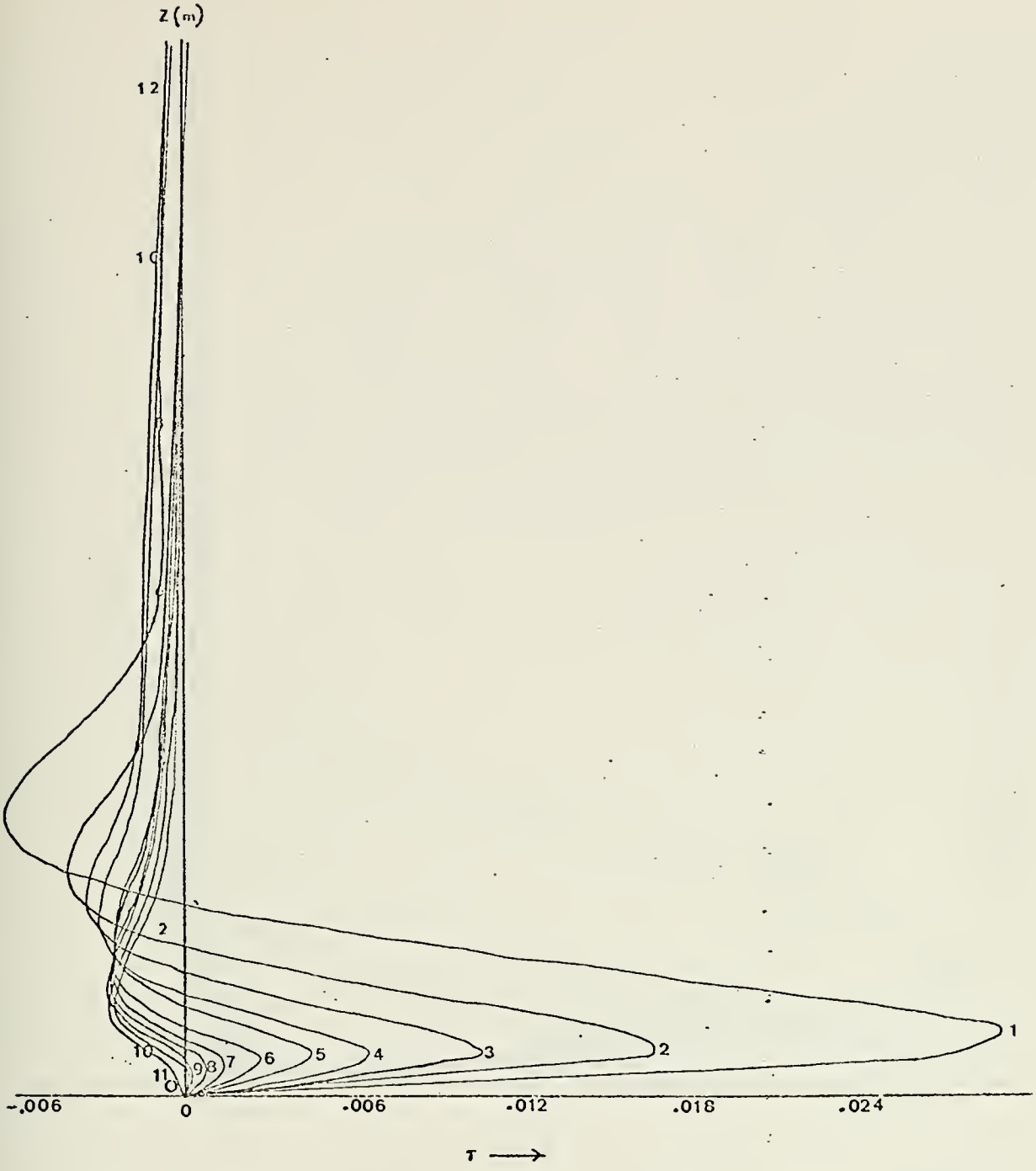

Figure 3. Distribution of the wave-caused stress (τ in $m^2 sec^2$) with height for $U_* = 0.02$ m/sec, $\nu = 0.240$ m^2/sec, $z_o = 0.0001$m and k equal, respectively, to: 1) 0.050, 2) 0.075, 3) 0.100, 4) 0.125, 5) 0.150, 6) 0.175, 7) 0.200, 8) 0.225, 9) 0.250, 10) 0.275, 11) 0.300.

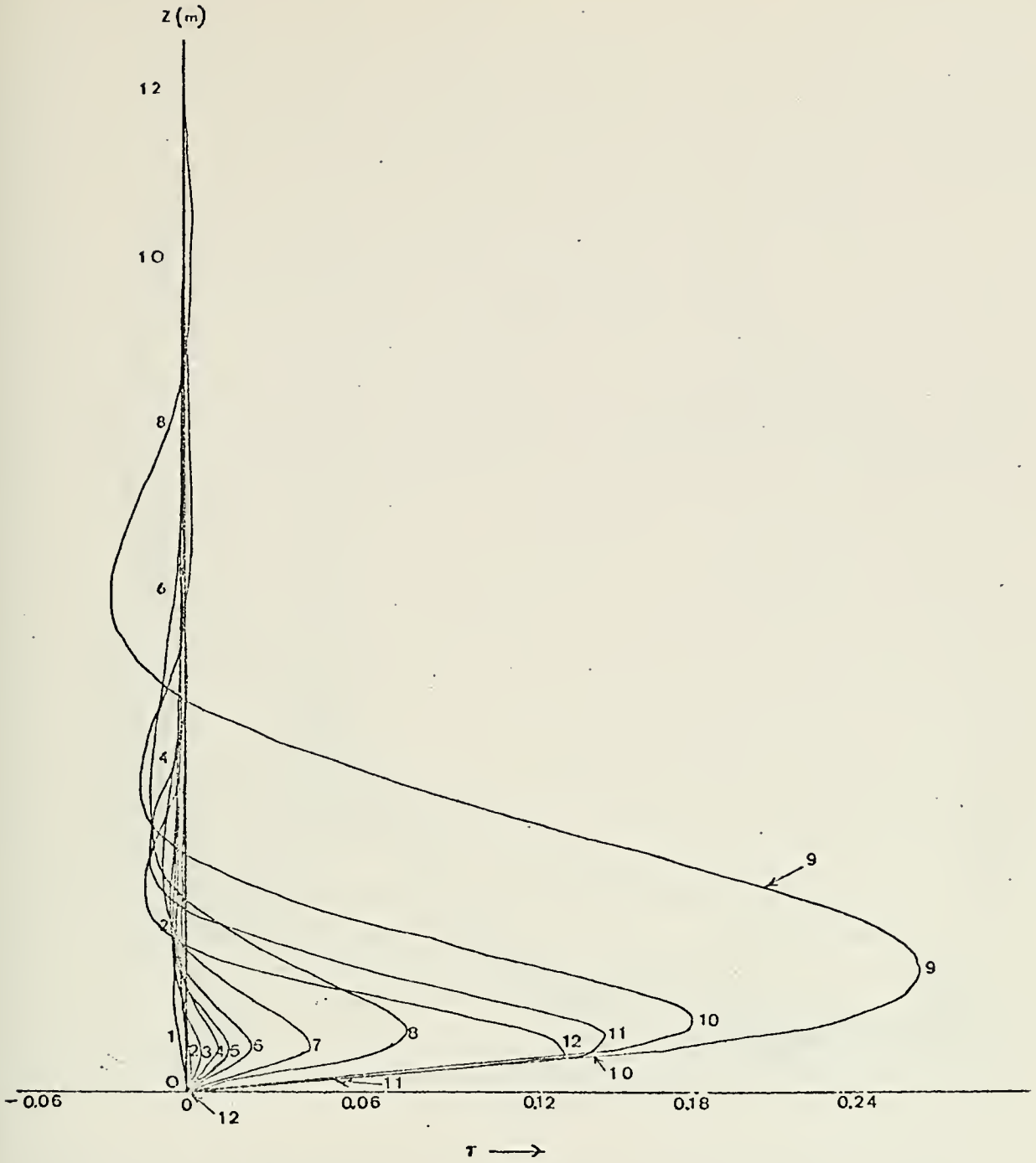

Figure 4. Distribution of the wave-caused stress (τ in m^2/sec^2) with height for $k = 0.200 m^{-1}$, $\nu = 0.240\ m^2/sec$, $z_o = 0.0001m$, and U_* equal, respectively, to: 1) 0,01, 2) 0.02, 3) 0.04, 4) 0.06, 5) 0.08, 6) 0.10, 7) 0.15, 8) 0.20, 9) 0.25, 10) 0.30, 11) 0.35, 12) 0.40. The arrows indicate the height of the critical level and the identifying dynamic velocity.

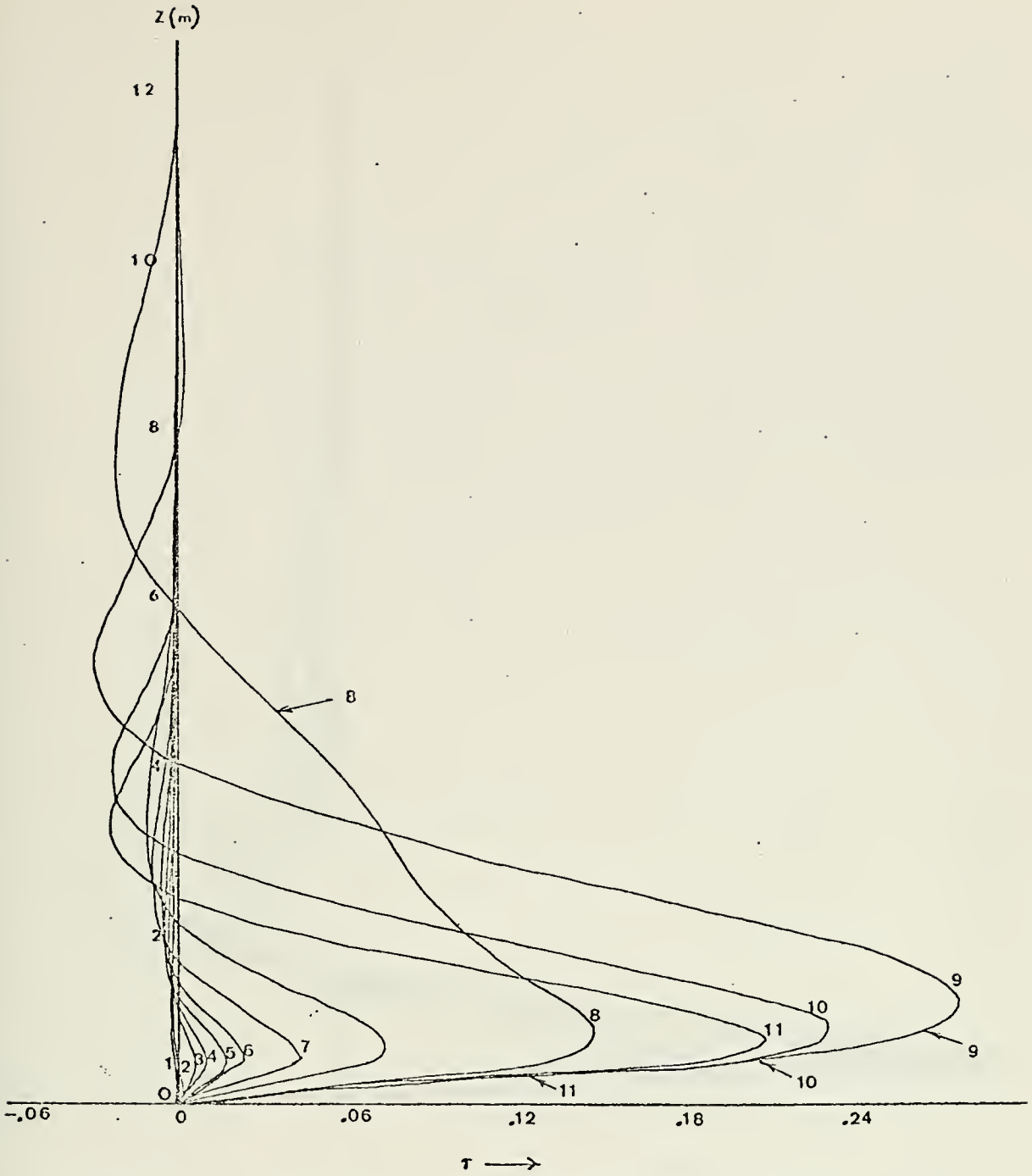

Figure 5. Distribution of the wave-caused stress (τ in m^2/sec^2) with height for $k = 0.20m^{-1}$, $\nu = 0.240$ m^2/sec, $z_o = 0.00428\ U_*^2$ and U_* equal, respectively, to: 1) 0.01, 2) 0.02, 3) 0.04, 4) 0.06, 5) 0.08, 6) 0.10, 7) 0.15, 8) 0.20, 9) 0.25, 10) 0.30, 11) 0.35, 12) 0.40. The arrows indicate the height of the critical level and the identifying dynamic velocity.

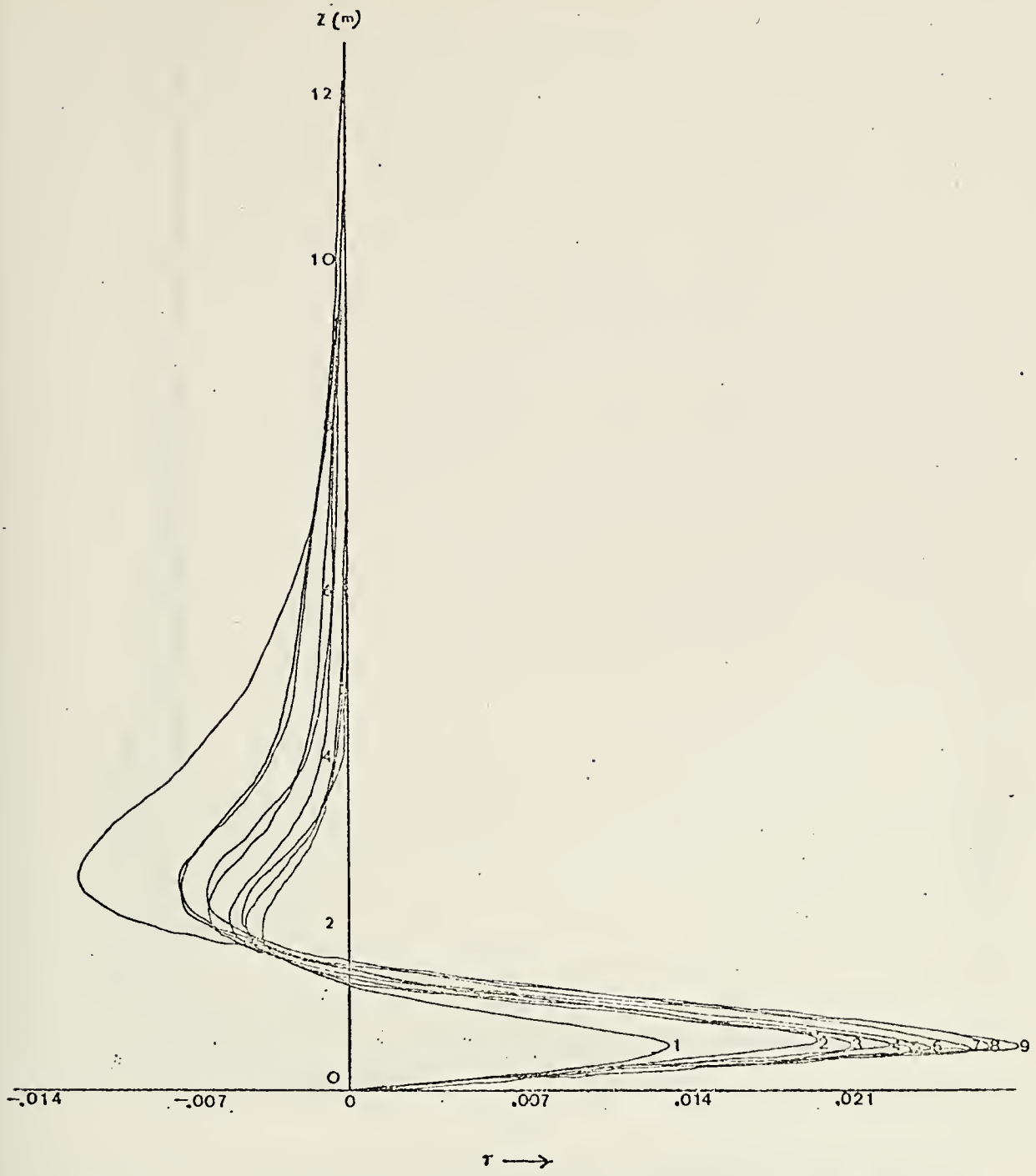

Figure 6. Distribution of the wave-caused stress (τ in m^2/sec^2) with height for $U_* = 0.100$ m/sec, $k = 0.200\ m^{-1}$, $\nu = 0.240 m^2/sec$ and z_o equal, respectively, to: 1) 0.1, 2) 0.01, 3) 0.001, 4) 0.0005, 5) 0.0001, 6) 0.00005, 7) 0.00001, 8) 0.000005, 9) 0.000001.

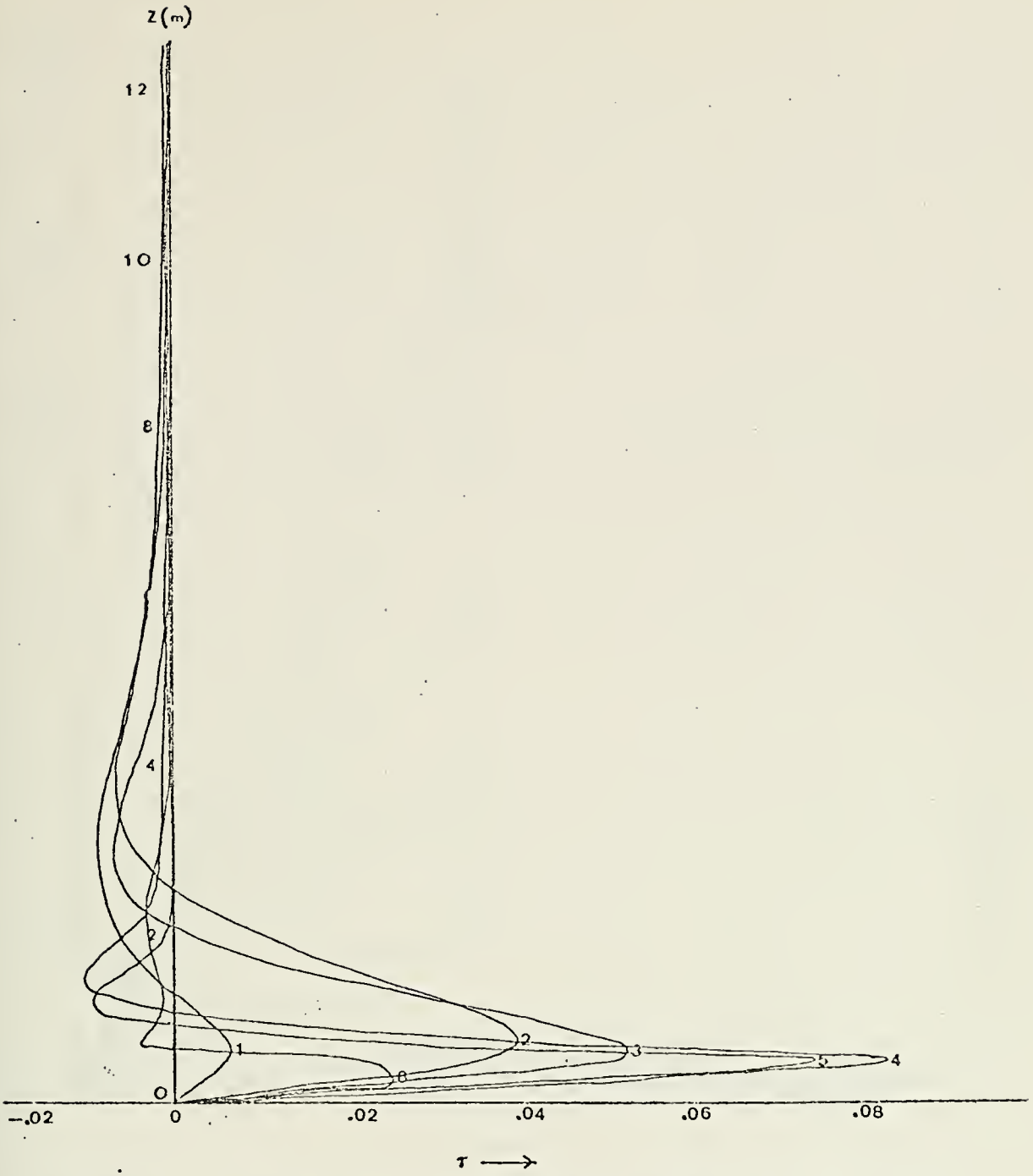

Figure 7. Distribution of the wave-caused stress (τ in m^2/sec) with height for $k = 0.200\ m^{-1}$, $U_* = 0.100$ m/sec, $z_o = 0.0001$m, and ν equal, respectively, to: 1) 1.100, 2) 0.200, 3) 0.110, 4) 0.020, 5) 0.011, 6) 0.002.

Figure 8. Variation of the turbulent coefficient with height, respectively, to: 1) decreasing, 2) increasing to 5m, 3) increasing to 10m, 4) increasing to 15m, 5) increasing to 20m, 6) increasing to 25m.

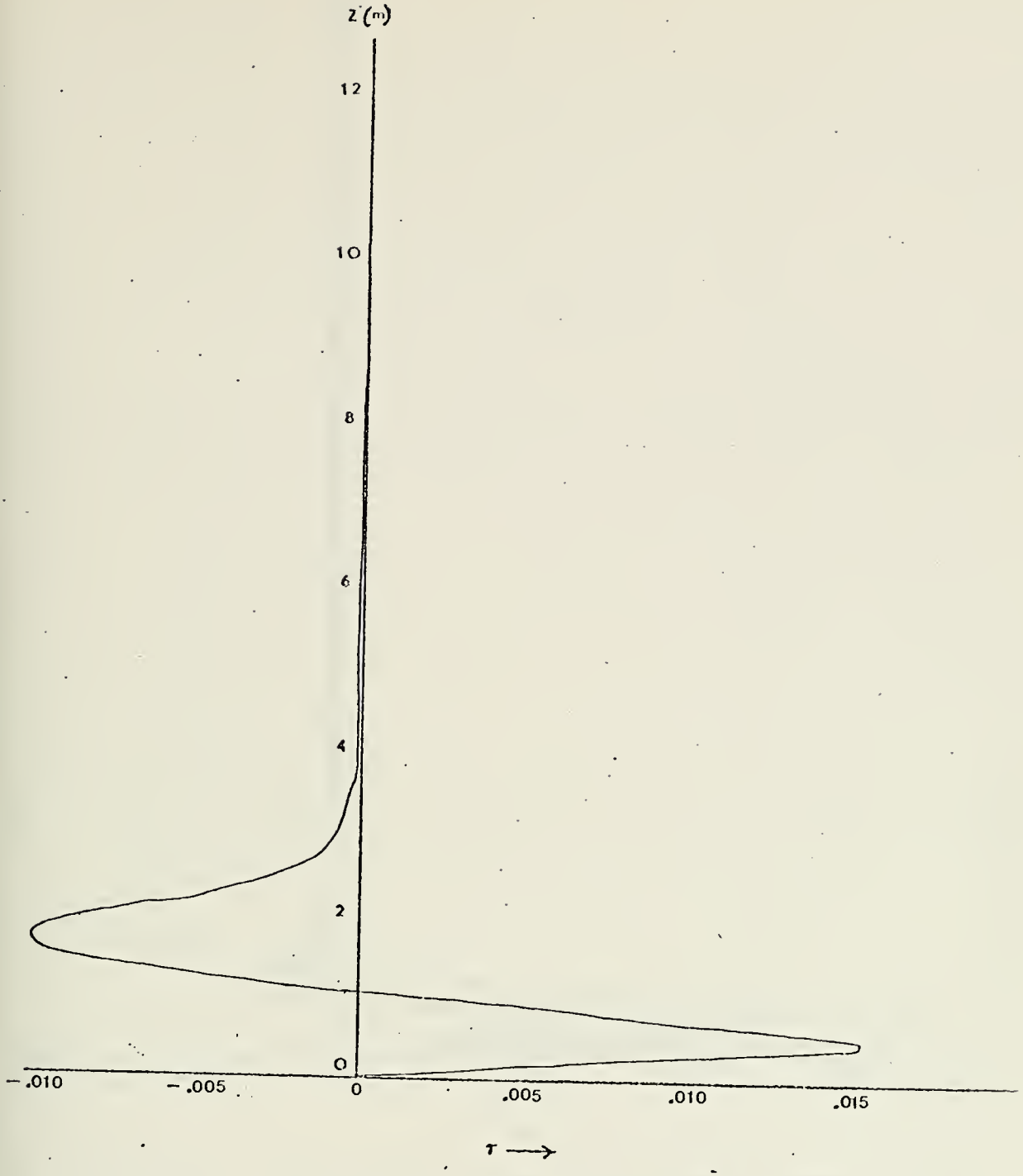

Figure 9. Distribution of the wave-caused stress (τ in m^2/sec^2) with height for $U_* = 0.100$ m/sec, $k = 0.200\ m^{-1}$, $z_o = 0.0001$m and ν decreasing with height.

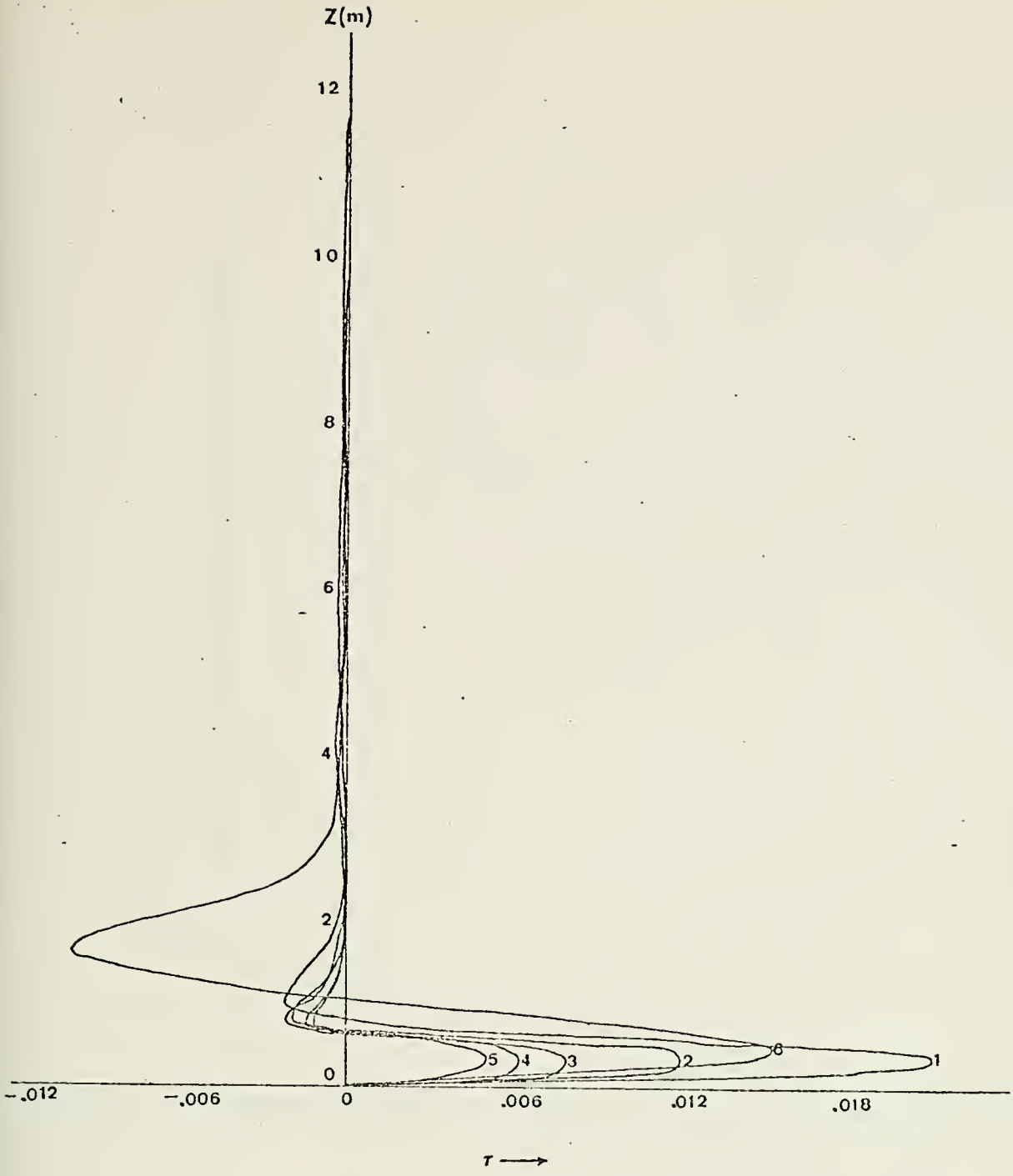

Figure 10. Distribution of the wave-caused stress (τ in m^2/sec^2) with height for $U_* = 0.100m/sec$, $k = 0.200m^{-1}$, $z_o = 0.0001m$ and ν increasing with height, respectively, to: 1) 5m, 2) 10m, 3) 15m, 4) 20m, 5) 25m. Curve 6) is the case of constant ν with the same U_*, k and z_o values.

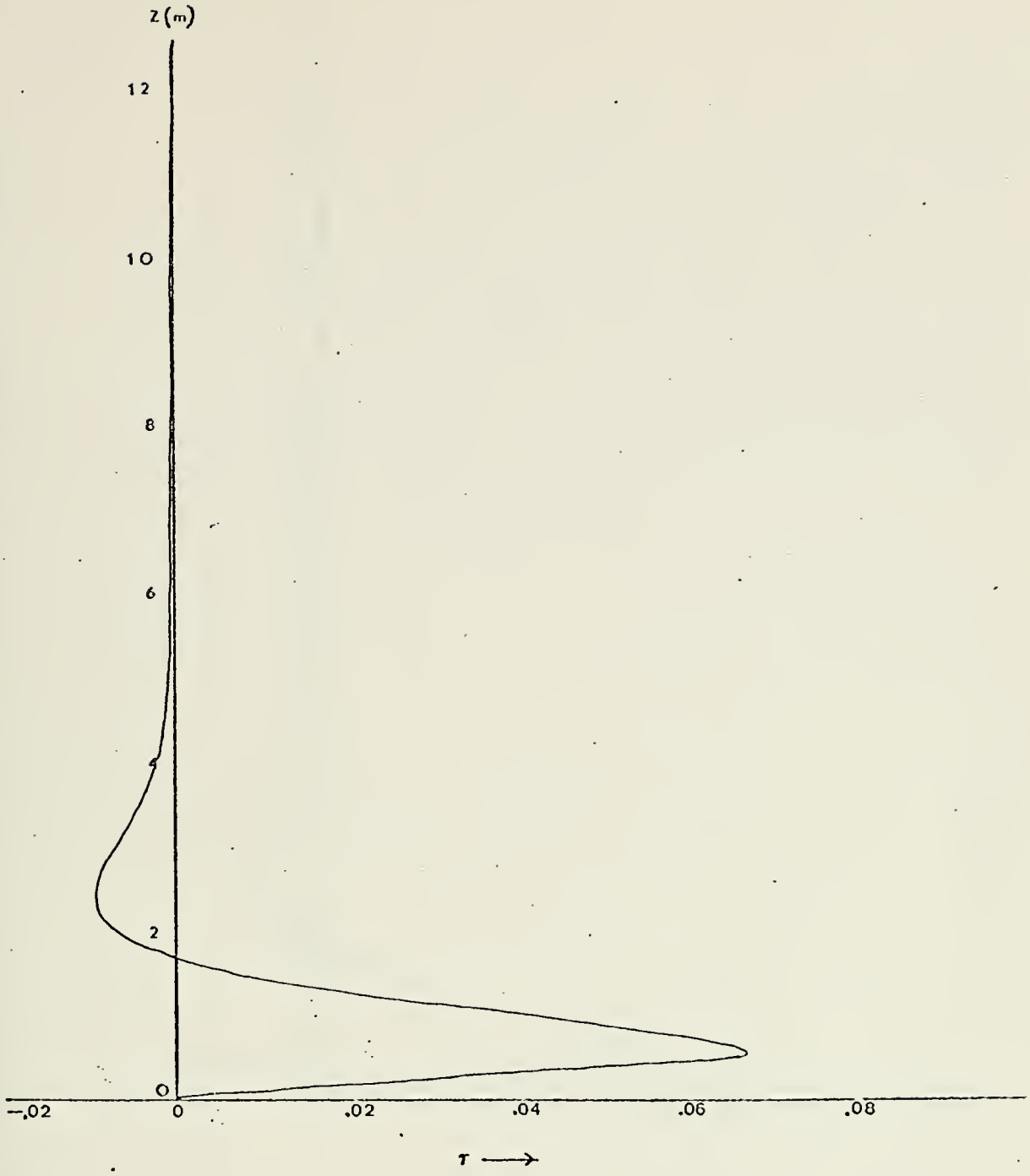

Figure 11. Distribution of the wave-caused stress (τ in m^2/sec^2) with height for $k = 0.179 m^{-1}$, $U_* = 0.200$ m/sec, $z_o = 0.003280$m, and $\nu = 0.240 m^2/sec^2$.

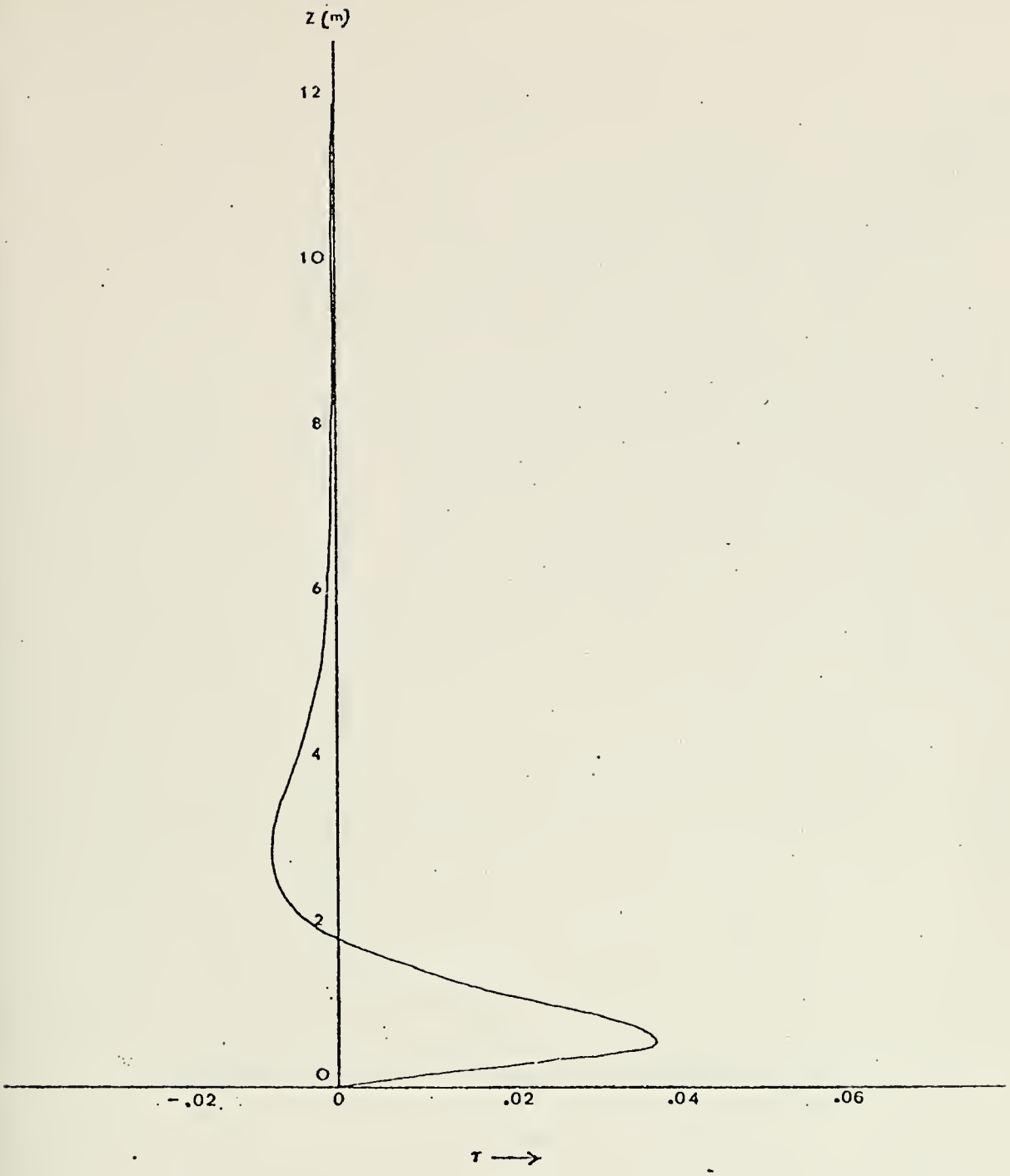

Figure 12. Distribution of the wave-caused stress (τ in m^2/sec^2) with height for $k = 0.273m^{-1}$, $U_*^2 = 0.167m/sec$, $z_o = 0.000079m$, and $\nu = 0.240m^2/sec^2$.

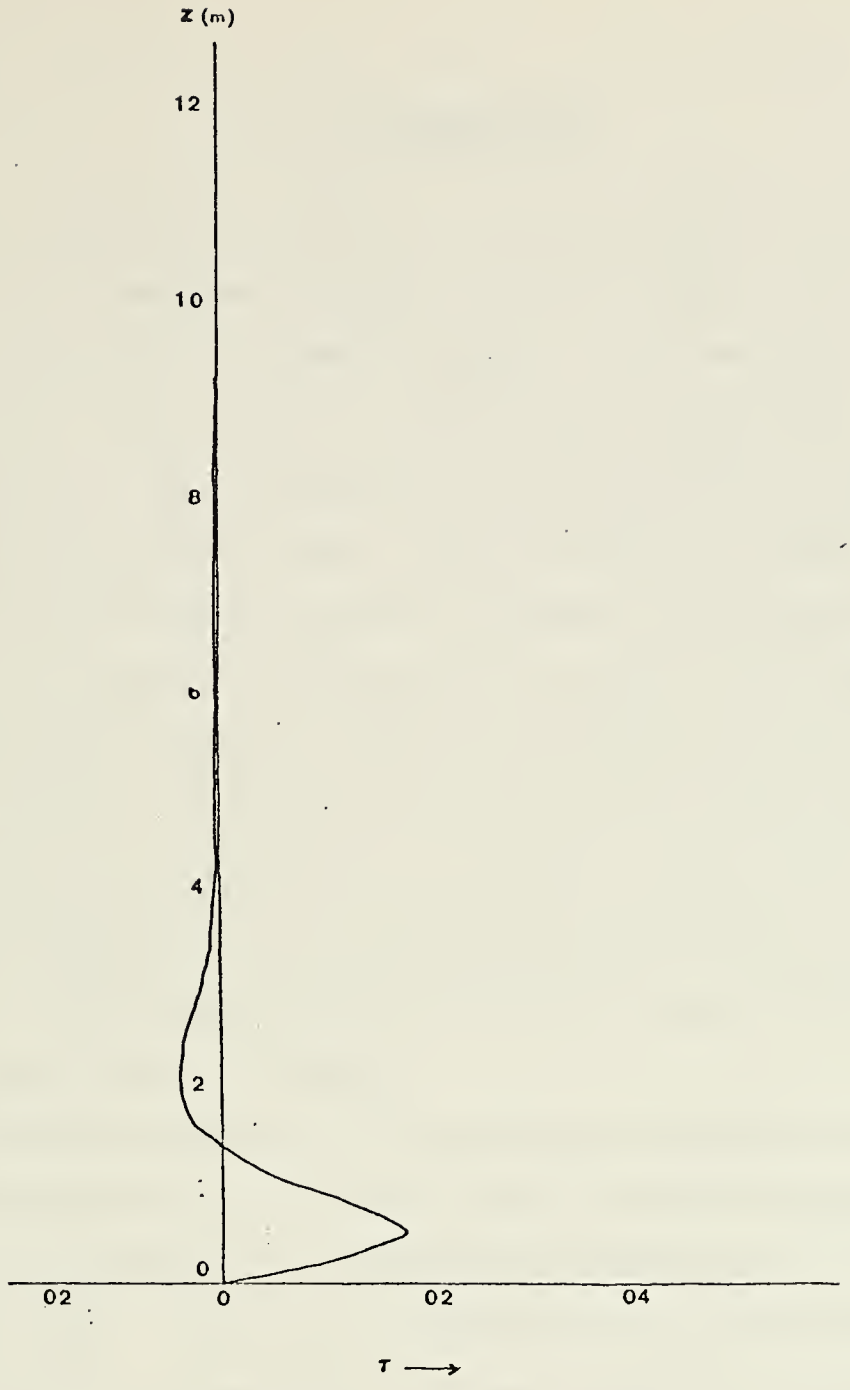

Figure 13. Distribution of the wave-caused stress (τ in m^2/sec^2) with height for $k = 0.273m^{-1}$, U_{*2}= 0.121m/sec, z_o = 0.000130m, and ν=0.240 m^2/sec^2.

VI. CONCLUSIONS

The Reynolds wave stress of the perturbation-velocity field in the atmospheric near water layer above waves has been obtained from a numerical model. The resultant Reynolds stress can be used to compute the energy which is transferred by the average motion of the air to the wave fluctuations and vice versa. Thus a positive stress indicates the wind energy maintains the wave fluctuations signifying a transfer of energy from the wind to the waves.

The maximum Reynolds stress and greatest energy transfer was found to exist for the largest mean wind profile (largest U_* and smallest z_o), the lowest wave numbers and a turbulent coefficient of approximately 0.020 $m^2 sec$. In addition, the maximum stress occurred at approximately one meter above the wave surface.

A striking result is the increase in the magnitude of the Reynolds stress as the mean wind velocity approaches that of the wave phase speed in the lowest levels of the boundary layer. For those cases where the critical level occurs in the region of the maximum stress fluctuations there is a significant increase in the magnitude of the stress. Thus the energy is greatest when wave velocity is close to the mean wind velocity in the lower levels.

Another significant result is the change which occurred in the stress profile when the turbulent coefficient was

allowed to vary with height. The net effect of this change is a decrease in the total energy transfer.

The comparison of numerically generated velocities and stresses with those of measured data yielded a very high degree of correlation. These results will justify future numerical research and data collection to provide new insights into the air-sea energy transfers. Specifically, the correlation of a numerical model with measured wind data could determine the characteristics of the turbulent coefficient due to the wave-caused motion. Concurrent studies being conducted by Aurand (1973) and Stricker (1973) may be considered as sources for additional data to correlate the statistically and numerically derived stress patterns.

APPENDIX A

BAROTROPIC INSTABILITY TEST

Neuman (1969) considered a simple barotropic numerical model. The object of the test was to determine the growth rate as a function of the wave number. The similarity between the present study and that of Neuman allowed for a check of the present model for the special case of no friction.

However, to accomplish the check, several modifications were made to the present model. These are:

$$A(z,0) = \cos\left(\frac{\pi y}{H}\right) \text{ , and}$$

$$\nu(z) = 0.$$

The mean wind velocity profile is given by:

$$U(z) = -U_o \tanh\left(y/y_o\right) \qquad \text{(A1)}$$

as shown in figure 14.

The procedure required marching the calculations forward in time until the growth rate stabilized. The point of maximum Reynolds stress for three different times were then compared. The magnitude of the stress at these points was found to be growing exponentially, as was expected.

As an additional check, the growth rate of the Reynolds stress was evaluated and compared to the growth rate as given by the function:

$$\exp\left(\frac{2U_o n}{y_o}\right)t \ . \qquad \text{(A2)}$$

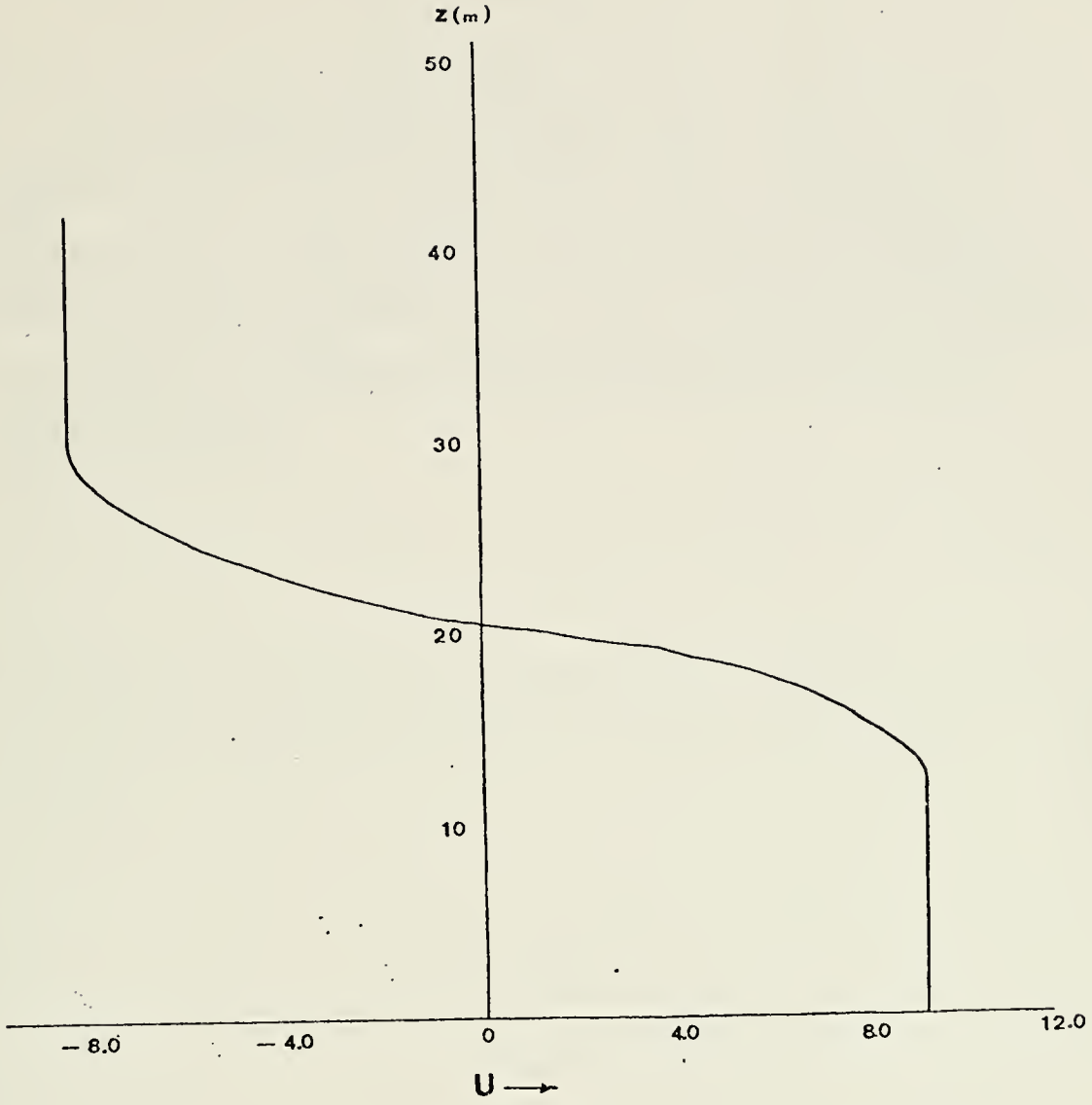

Figure 14. Mean wind profile for $U = -U_o \tanh(y/y_o)$, (m/sec).

In this case the stress at the maximum point was equated to (A2) and the equation solved for n using:

$$U_o = 9.0 \text{ m/sec} ,$$

$$y_o = 4.0\text{m} .$$

The resultant growth rate was 0.181. This is more accurate than that of Neuman who found a growth rate of 0.160, but it is less than that of Betchov and Criminale (1967) who set the rate at n = 0.19. The latter difference is because the present solution has been solved with a finite boundary.

APPENDIX B

EXAMINATION OF THE VISCOSITY TERMS

In this test the initial field of the cosine stream function amplitudes was computed utilizing equation (3.2). At this point the mean wind and phase speed were set to zero. Then the forecast equations were marched forward until a steady state was reached.

These numerical values were then compared with the analytical values derived from the solution of the equation:

$$A_{zzzz} + 2A_{zz} + A = 0 \ . \qquad \text{(B1)}$$

The boundary conditions utilized in the solution of (B1) are similar to those given by (3.4) and (3.6). These conditions are:

$$A(0) = 2c \ , \ A_z(0) = -2kc \ ,$$

$$A(H) = A_z(H) = 0 \ .$$

The solution of (B1) is given by:

$$A(z) = c_1 \sin(kz) + c_2 \cos(kz) + c_3 \, kz \sin(kz) + c_4 \, kz \cos(kz) \ , \qquad \text{(B2)}$$

where:

$$c_1 = \frac{1}{k}\,[A_z(0) - c_4\,k]\ ,$$

$$c_2 = A\ ,$$

$$c_3 = -\frac{1}{Hk\,\sin\,(Hk)}[A_z(0)\sin(Hk) + A(0)\cos(Hk) + c_4\,\sin(Hk) + c_4\,Hk\,\cos\,(Hk)]\ ,$$

$$c_4 = \frac{H\,\sin\,(Hk)}{\sin^2(Hk) - H^2k^2}\left([A(0) + \frac{A_z(0)}{Hk}]\sin(Hk) + [\frac{A(0)}{H} + A(0)k\,\cot(Hk)]\,\cos(Hk)\right)\ .$$

The comparison of the numerical results with the analytical results derived from (B2) indicated that the minimum occurred at the same height for both cases. However, the magnitude of the numerical minimum was smaller than that of the analytical results.

APPENDIX C

EXAMINATION OF THE CASE OF NO MEAN WIND

Yefimov and Pososhkov (1970) derived an analytic solution to the forecast equations (2.15) and (2.16) for the special case U = 0. This solution is given by:

$$\tau = -\overline{u'w'} = -\alpha e^{-2zk} + \alpha e^{-zk/\sqrt{2\alpha}} \cos\left(\frac{zk}{\sqrt{2\alpha}}\right) , \qquad (C1)$$

where:

$$\alpha = \frac{\nu k}{c} .$$

The condition U = 0 was established and the numerical solutions of (2.15) and (2.16) were computed to a steady state condition. The results of the analytical and numerical calculations of stress were compared for several different wave numbers and for different values of the turbulent exchange coefficient.

The results of the stress obtained by both methods were very similar. In all cases compared the analytical stress reached a minimum at a lower height and somewhat smaller magnitude than the numerically derived stress. This discrepancy, however, has been primarily attributed to the scale of the grid increment.

APPENDIX D

EXAMINATION OF THE RICHTMYER SCHEME

This test was devised solely to test the method of solving equations as given by Richtmyer (1957). The test was conducted by equating the right hand side terms of equation (2.15) to sin $(\frac{\pi z}{w})$ where $w = (H-3)\Delta z$. The result is:

$$(\frac{\partial^2}{\partial z^2} - k^2) \frac{\partial A}{\partial t} = \sin (\frac{\pi z}{w}) ,$$

and upon solution yields:

$$A = \frac{-1}{[(\frac{\pi}{w})^2 + k^2]} \Delta t . \qquad \text{(D1)}$$

The numerical solution was marched forward one complete time step. Then the minimum value of the stream function amplitude, A(z,t), was compared with the value derived from (D1). The result was a comparison of the values to within three percent of the difference.

APPENDIX E

EVALUATION OF ANALYZED DATA

Davidson and Frank (1973) reported observed values of wave heights and velocity fluctuations at two levels above the waves. The results from their spectral and joint probability density function, conditional mean function (JPDF-CMF) analyses are shown in Figures 15 and 16.

The velocity variance spectra graphs show plots of $n \cdot \phi(n)$ vs. $\ln(n)$ where n is the frequency of the wave in Hz. The area under the significant spikes of the curve (shaded areas of Figure 15) can be used to determine the value of the square of the wave-caused velocity fluctuation (u'^2 or w'^2). These areas may be computed by:

$$\text{Area} = n \cdot \phi(n) \cdot \Delta \ln(n) , \qquad \text{(E1)}$$

where $\Delta \ln(n)$ is defined at the significant peak.

The velocity cospectra graphs (Figure 15) are similar to those above but the area in this case is indicative of the wave-caused Reynolds stress ($\overline{u'w'}$). These results have been presented in Table III for comparison.

Davidson and Frank (1973) also presented phase-amplitude results for the same data as above. These results (Figure 16), which may be interpreted directly, are shown in Table III for comparison.

The numerical maximum amplitude has been computed from the steady state values of the stream function amplitude by:

$$u' = (A_z^2 + B_z^2)^{1/2} \qquad \text{(E2)}$$

and

$$w' = k(A^2 + B^2)^{1/2} \qquad \text{(E3)}$$

which follow as a result from equations (2.11) and (2.14). The numerical results were computed with the small wave slope assumption where ak = 0.1. However, this exact condition is not normally met in nature. Therefore, the values obtained from equations (E2) and (E3), as well as the numerically derived Reynolds stress, must be scaled to reflect the actual wave slope.

The calculation of a scaling factor first involved the determination of the actual amplitude (a_D). This may be interpreted directly from the "waves" diagram in Figure 16. The amplitude used for the numerical calculations may be computed by:

$$a_N = \frac{0.1}{k}$$

The resulting velocity scaling factor (Fs) may now be expressed by:

$$Fs = \frac{a_D}{a_N}, \qquad \text{(E4)}$$

and the quadratic stress scaling factor (Fq) by:

$$Fq = \frac{a_D^2}{a_N^2} . \qquad \text{(E5)}$$

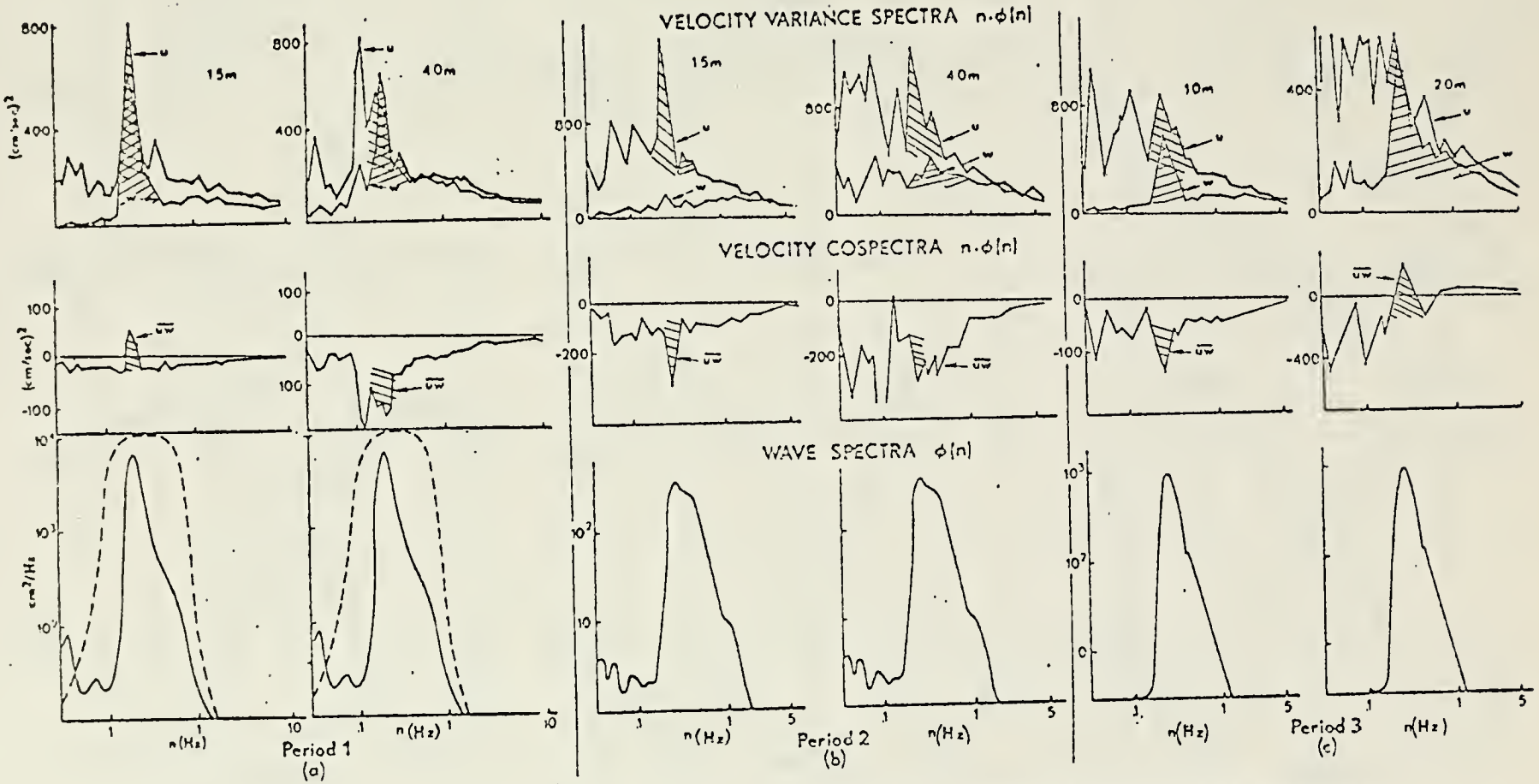

Figure 15. Velocity variance spectra, velocity cospectra and wave spectra taken from [illegible] and Frank (1973).

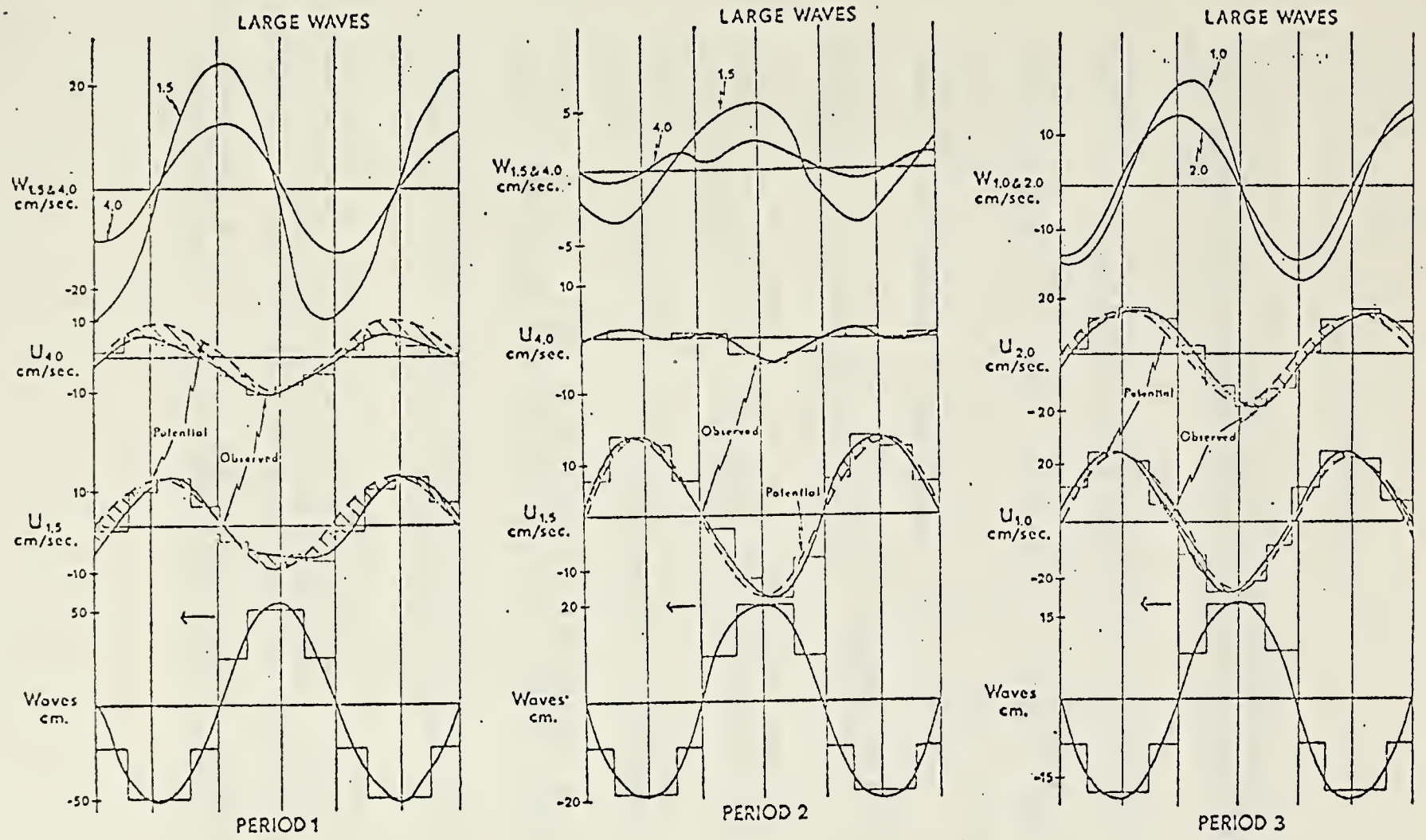

Figure 16. Phase-amplitude results for large waves taken from Davidson and Frank (1973).

LIST OF REFERENCES

1. Aurand, D. T., 1973: Wave-related velocity fluctuations over ocean waves as measured from Flip during BOMEX. M.S. Thesis, Naval Postgraduate School, Monterey, California, 50 pp.

2. Benjamin, T. B., 1959: "Shearing flow over a wavy boundary." Journal of Fluid Mechanics, 6, 161-205.

3. Betchov, R., and Criminale, W., 1967: Stability of Parallel Flows, Academic Press, New York, N.Y., 330 pp.

4. Davidson, K. L. and Frank, A. J., 1973: "Wave-related fluctuations in the airflow over natural waves." Journal of Physical Oceanography, 3, 1, 102-119.

5. Hill, M. N., 1962: The Sea, Ideas and Observations on Progress in the Study of the Seas. Interscience Publishers, Inc., New York, p. 57.

6. Kraus, E. B., 1968: "What do we not know about the sea-surface wind stress." Bulletin of the American Meteorological Society, 49, 3, 247-253.

7. Miles, J. W., 1957: "On the generation of surface waves by shear flows." Journal of Fluid Mechanics, 3, 185-204.

8. Newman, R. L., 1969: A Theoretical Investigation of the Structure of Easterly Waves. M.S. Thesis, Naval Postgraduate School, Monterey, California, 67 pp.

9. Phillips, O. M., 1957: "On the generation of waves by turbulent wind." Journal of Fluid Mechanics, 2, 417-445.

10. Reynolds, W. C. and Hussain, A.K.M.F., 1972: "The mechanics of an organized wave in turbulent shear flow. Part 3. Theoretical models and comparisons with experiments." Journal of Fluid Mechanics, 54, 263-288.

11. Richtmyer, R. D., 1957: Difference Methods for Initial Value Problems. Interscience Publishers, Inc., New York.

12. Stricker, R. J., 1973: Normalized Spectra of Turbulent Fluctuations over Ocean Waves. M.S. Thesis, Naval Postgraduate School, Monterey, California, 65 pp.

13. Yefimov, V. V., 1970: "On the structure of the wind velocity field in the atmospheric near-water layer and the transfer of wind energy to sea waves." Atmospheric and Oceanic Physics, 6, 10, 1043-1958, translated by McIntosh, J.D.L.

14. Yefimov, V. V. and Pososhkov,V. L., 1970: "The dynamics of wave disturbances of the atmospheric boundary layer by swell." Atmospheric and Oceanic Physics, 6, 6, 617-628, translated by Findlay, J.

INITIAL DISTRIBUTION LIST

		No. Copies
1.	Defense Documentation Center Cameron Station Alexandria, Virginia 22314	2
2.	Library, Code 0212 Naval Postgraduate School Monterey, California 93940	2
3.	Dr. R. T. Williams, Code 51Wu Department of Meteorology Naval Postgraduate School Monterey, California 93940	5
4.	Lieutenant Commander B. C. Stauffer Fleet Numerical Weather Facility Naval Postgraduate School Monterey, California 93940	4
5.	Naval Weather Service Command Washington Navy Yard Washington, D. C. 20390	1
6.	Officer in Charge Environmental Prediction Research Facility Naval Postgraduate School Monterey, California 93940	1
7.	Commanding Officer U. S. Fleet Weather Central COMNAVMARIANAS, Box 12 FPO San Francisco, California 96630	1
8.	Commanding Officer Fleet Weather Facility P. O. Box 85 Naval Air Station Jacksonville, Florida 32212	1
9.	Commanding Officer U. S. Fleet Weather Facility Box 72 FPO New York, New York 09510	1

10. Commanding Officer — 1
Fleet Numerical Weather Central
Naval Postgraduate School
Monterey, California 93940

11. Commanding Officer — 1
U. S. Fleet Weather Central
Box 110
FPO San Francisco, California 96610

12. Commanding Officer — 1
U. S. Fleet Weather Central
Box 31
FPO New York, New York 09540

13. Commanding Officer — 1
U. S. Fleet Weather Facility, Box 30
FPO San Francisco, California 96652

14. AFCRL - Research Library — 1
L. G. Hanscom Field
Attn: Nancy Davis/Stop 29
Bedford, Massachusetts 01730

15. Director, Naval Research Laboratory — 1
Attn: Tech. Services Information Officer
Washington, D. C. 20390

16. American Meteorological Society — 1
45 Beacon Street
Boston, Massachusetts 02128

17. Department of Meteorology — 3
Code 51
Naval Postgraduate School
Monterey, California 93940

18. Department of Oceanography — 1
Code 58
Naval Postgraduate School
Monterey, California 93940

19. Office of Naval Research — 1
Department of the Navy
Washington, D. C. 20360

20. Commander, Air Weather Service — 2
Military Airlift Command
United States Air Force
Scott Air Force Base, Illinois 62226

21. Atmospheric Sciences Library 1
National Oceanic and Atmospheric Administration
Silver Spring, Maryland 20910

22. Professor Victor Starr 1
Department of Meteorology
M.I.T.
Cambridge, Massachusetts 03139

23. Dr. J. Pedlosky 1
Department of Geophysical Sciences
University of Chicago
Chicago, Illinois 60637

24. Dr. Joanne Simpson 1
Experimental Meteorology Branch
National Oceanic and Atmospheric Administration
Coral Gables, Florida 33124

25. Dr. V. Jurcec 1
Boskoviceva 31/111
41000 Zagreb
Yugoslavia

26. Dr. G. C. Asnani 1
Observatory
Poona 5, India

27. National Center for Atmospheric Research 1
Box 1470
Boulder, Colorado 80302

28. Dr. T. N. Krishnamurti 1
Department of Meteorology
Florida State University
Tallahassee, Florida 32306

29. Dr. Fred Shuman, Director 1
National Meteorological Center
National Oceanic and Atmospheric Administration
Suitland, Maryland 20390

30. Dr. J. Smagorinsky, Director 1
Geophysical Fluid Dynamics Laboratory
Princeton University
Princeton, New Jersey 08540

31. Professor N. A. Phillips 1
Department of Meteorology
M.I.T.
Cambridge, Massachusetts 02139

32. Professor J. G. Charney 1
54-1424
M.I.T.
Cambridge, Massachusetts 02139

33. Dr. F. Sanders 1
Department of Meteorology
M.I.T.
Cambridge, Massachusetts 02139

34. Professor K. Ooyama 1
Department of Meteorology
New York University
University Heights
New York, New York 10453

35. Dr. C. E. Palmer 1
Institute of Geophysics
UCLA
Los Angeles, California 90024

36. Dr. M. G. Wurtele 1
Department of Meteorology
UCLA
Los Angeles, California 90024

37. Dr. A. Arakawa 1
Department of Meteorology
UCLA
Los Angeles, California 90024

38. Professor H. Riehl 1
Institut fuer Meteorologie
Freie Universitaet Berlin
Berlin, West Germany

39. Dr. G. Haltiner, Chairman 1
Department of Meteorology, Code 51Ha
Naval Postgraduate School
Monterey, California 93940

40. Dr. R. L. Haney 1
Department of Meteorology, Code 51Hy
Naval Postgraduate School
Monterey, California 93940

41. Dr. R. Elsberry 1
Department of Meteorology, Code 51Es
Naval Postgraduate School
Monterey, California 93940

42. Dr. C. P. Chang — 1
Department of Meteorology, Code 51Cj
Naval Postgraduate School
Monterey, California 93940

43. Dr. R. Renard — 1
Department of Meteorology, Code 51Rd
Naval Postgraduate School
Monterey, California 93940

44. Dr. J. Galt — 1
Department of Oceanography, Code 58
Naval Postgraduate School
Monterey, California 93940

45. Dr. K. Davidson — 5
Department of Meteorology, Code 51Ds
Naval Postgraduate School
Monterey, California 93940

46. Dr. R. Alberty — 1
National Severe Storms Laboratory
1313 Halley Circle
Norman, Oklahoma 73069

47. Professor Peter J. Gierasch — 1
Space Sciences Building
Cornell University
Ithaca, New York 14850

48. Dr. Peter H. Stone — 1
Institute for Space Studies
2880 Broadway
New York, New York 10025

49. Dr. S. Piacsek — 1
Code 7750
Naval Research Laboratory
Washington, D. C. 20390

50. Dr. E. N. Lorenz — 1
Department of Meteorology
M.I.T.
Cambridge, Massachusetts 02139

51. Dr. D. Houghton — 1
Department of Meteorology
University of Wisconsin
Madison, Wisconsin 53706

52. Dr. S. K. Kao 1
Department of Meteorology
University of Utah
Salt Lake City, Utah 84112

53. Dr. A. P. Ingersoll 1
Division of Geological and Planetary Sciences
California Institute of Technology
Pasadena, California 91109

54. Mrs. O. Haney 1
Environmental Prediction Research Facility
Naval Postgraduate School
Monterey, California 93940

55. Dr. J. Wallace 1
Department of Atmospheric Sciences
University of Washington
Seattle, Washington 98105

56. Dr. J. Holton 1
Department of Atmospheric Sciences
University of Washington
Seattle, Washington 98105

57. Dr. J. Young 1
Department of Meteorology
University of Wisconsin
Madison, Wisconsin 53706

58. Dr. T. Ogura 1
Laboratory for Atmospheric Research
University of Illinois
Urbana, Illinois 61801

59. Dr. Y. Sasaki 1
Department of Meteorology
University of Oklahoma
Norman, Oklahoma 73069

60. Dr. J. Mahlman 1
Geophysical Fluid Dynamics Laboratory
Princeton University
Princeton, New Jersey 08540

61. Dr. R. Alexander 1
The Rand Corporation
1700 Main Street
Santa Monica, California 90406

62. Dr. W. L. Gates 1
The Rand Corporation
1700 Main Street
Santa Monica, California 90406

63. Dr. S. Rosenthal 1
National Hurricane Research Laboratory
P. O. Box 8265
University of Miami Beach
Coral Gables, Florida 33124

64. Mr. Tom Baxter 1
Environmental Prediction Research Facility
Naval Postgraduate School
Monterey, California 93940

65. Lieutenant Commander A. J. Frank 1
RVAH-3
Naval Air Station
Albany, Georgia 31701

66. Dr. V. V. Yefimov 1
Academy of Sciences of the
USSR Marine Hydrophysical Institute
Moscow, USSR

67. Dr. R. E. Davis 1
University of California at San Diego
San Diego, California 92037

68. Dr. J. W. Miles 1
University of California at San Diego
San Diego, California 92037

69. Dr. O. M. Phillips 1
John Hopkins University
Baltimore, Maryland 21218

70. Dr. W. C. Reynolds 1
Department of Mechanical Engineering
Stanford University
Palo Alto, California 94305

71. Dr. D. J. Portman 1
Department of Meteorology
University of Michigan
Ann Arbor, Michigan 48105

72. Professor T. Green 1
Department of Meteorology
University of Wisconsin
Madison, Wisconsin 53706

Security Classification

DOCUMENT CONTROL DATA - R & D

(Security classification of title, body of abstract and indexing annotation must be entered when the overall report is classified)

ORIGINATING ACTIVITY *(Corporate author)*

Naval Postgraduate School
Monterey, California 93940

2a. REPORT SECURITY CLASSIFICATION

Unclassified

2b. GROUP

REPORT TITLE

Application of a Theoretical Model to Velocity Fields Observed Over Water Waves

DESCRIPTIVE NOTES *(Type of report and, inclusive dates)*

Master's Thesis; March 1973

AUTHOR(S) *(First name, middle initial, last name)*

Barry C. Stauffer

REPORT DATE	7a. TOTAL NO. OF PAGES	7b. NO. OF REFS
March 1973	66	14

CONTRACT OR GRANT NO.

PROJECT NO.

9a. ORIGINATOR'S REPORT NUMBER(S)

9b. OTHER REPORT NO(S) *(Any other numbers that may be assigned this report)*

DISTRIBUTION STATEMENT

Approved for public release; distribution unlimited.

SUPPLEMENTARY NOTES

12. SPONSORING MILITARY ACTIVITY

Naval Postgraduate School
Monterey, California 93940

ABSTRACT

A theoretical model is developed for the wind velocity field in the atmospheric near-water layer above ocean waves. A turbulent exchange coefficient due to the wave-caused velocity fluctuations is introduced into the equations to account for the corresponding turbulent nature of the motion and the resulting energy fluxes. The equations of motion for air are derived in a manner to allow for variation of the turbulent exchange coefficient with height. A stream function is introduced and a numerical solution obtained by utilization of the Richtmyer method. The profiles of wave-caused Reynolds stresses and their resulting energy transfers are discussed and compared with observational data.

DD FORM 1 NOV 68 1473 (PAGE 1)

S/N 0101-807-6811

Security Classification

A-31406

KEY WORDS	LINK A		LINK B		LINK C	
	ROLE	WT	ROLE	WT	ROLE	WT
Reynolds stress						
turbulent exchange coefficient						
wave-caused velocity perturbations						
stream function						
turbulent velocity fluctuation						
dynamic velocity						
roughness length						
wave number						
vorticity						

Thesis 143226
S6779 Stauffer
c.1 Application of a theoretical model to velocity fields observed over water waves.